ADVANCED HEALTHCARE MATERIALS
www.advhealthmat.de

Functionalized Silk Vascular Grafts with Decellularized Human Wharton's Jelly Improves Remodeling via Immunomodulation in Rabbit Jugular Vein

Prerak Gupta, Gaurab Ranjan Chaudhuri, G. Janani, Manoj Agarwala, Debaki Ghosh, Samit K. Nandi, and Biman B. Mandal**

Cell-free polymeric tissue-engineered vascular grafts (TEVGs) have shown great promise towards clinical translation; however, their limited bioactivity and remodeling ability challenge this cause. Here, a novel cell-free bioresorbable small diameter silk TEVG system functionalized with decellularized human Wharton's jelly (dWJ) matrix is developed and successfully implanted as interposition grafts into rabbit jugular vein. Implanted TEVGs remain patent for two months and integrate with host tissue, demonstrating neo-tissue formation and constructive remodeling. Mechanistic analysis reveals that dWJ matrix is a reservoir of various immunomodulatory cytokines (Interleukin-8, 6, 10, 4 and tumor necrosis factor alpha (TNF-α)), which aids in upregulating M2 macrophage-associated genes facilitating pro-remodeling behavior. Besides, dWJ treatment to human endothelial cells upregulates the expression of functional genes (cluster of differentiation 31 (CD31), endothelial nitric oxide synthase (eNOS), and vascular endothelial (VE)-cadherin), enables faster cell migration, and elevates nitric oxide (NO) production leading to the in situ development of endothelium. The dWJ functionalized silk TEVGs support increased host cell recruitment than control, including macrophages and vascular cells. It endows superior graft remodeling in terms of a dense medial layer comprising smooth muscle cells and elevates the production of extracellular matrix proteins (collagen and elastin). Altogether, these findings suggest that dWJ functionalization imitates the usefulness of cell seeding and enables graft remodeling.

1. Introduction

Remodeling of tissue-engineered vascular grafts (TEVGs, all synthetic and natural grafts except native cellular blood vessels) predominantly relies on scaffold bioactivity, which is orchestrated by either incorporating diverse cell types or bioactive molecules.[1] Developing viable TEVGs using patient-specific vascular cells is a time-consuming process. It requires long-term in vitro expansion of autologous cells, scaffold seeding, and in vitro maturation under physiologically relevant dynamic culture conditions, thus limiting their clinical translation.[2] Alternatively, bone marrow mononuclear cells (BMMNCs) can be harvested in a time-efficient manner, which brings down the fabrication time from days to hours. BMMNCs have the inherent ability to recruit endogenous vascular cells, which facilitates in situ endothelialization and neo-tissue formation after transplantation.[3] Prior studies suggest that BMMNCs seeded in the vascular scaffolds assist in remodeling via paracrine communication.[3a,c] Monocyte chemoattractant protein-1 (MCP-1) secreted from mesenchymal stem cells (MSCs) was

P. Gupta, G. Janani, B. B. Mandal
Department of Biosciences and Bioengineering
Indian Institute of Technology Guwahati
Guwahati, Assam 781039, India
E-mail: biman.mandal@iitg.ac.in

G. R. Chaudhuri
Department of Plastic Surgery
R. G. Kar Medical College and Hospital
Kolkata, West Bengal 700004, India

M. Agarwala
Department of ENT and Faciomaxillary Surgery
GNRC Institute of Medical Sciences
Guwahati, Assam 781030, India

D. Ghosh, S. K. Nandi
Department of Veterinary Surgery and Radiology
West Bengal University of Animal and Fishery Sciences
Kolkata, West Bengal 700037, India
E-mail: drsknandi@wbuafscl.ac.in

B. B. Mandal
Centre for Nanotechnology
Indian Institute of Technology Guwahati
Guwahati, Assam 781039, India

B. B. Mandal
School of Health Sciences and Technology
Indian Institute of Technology Guwahati
Guwahati, Assam 781039, India

The ORCID identification number(s) for the author(s) of this article can be found under https://doi.org/10.1002/adhm.202100750

DOI: 10.1002/adhm.202100750

identified to be one of the signaling molecules involved in the former process.[3a] Functionalization of acellular (cell-free) vascular scaffolds with MCP-1 revealed comparable outcomes to BMMNCs-seeded scaffolds.[3a] From a translational perspective, acellular vascular grafts are expected to follow a shorter path than cell-seeded grafts. Hence a lateral shift is observed lately towards cell-free vascular grafts to expedite their clinical translation.[1,2]

Acellular TEVGs have shown promising outcomes in animal models and human clinical trials.[1,3c,4] Among biological grafts, autologous decellularized vessels (internal mammary artery[5] and umbilical artery[6]) are favored due to their regenerative potential and patency, but their sparsity limit clinical feasibility. Moreover, acellular xenografts pose the risk of immune rejection and disease transmission.[7] On the other side, polymeric grafts can be manufactured with high fidelity, which could be readily available for the patients and bypass the possibility of disease transmission. Prior reports show encouraging results for acellular polymeric grafts.[8] For example, human acellular vessels (HAVs) are the most advanced acellular vascular grafts that are developed by seeding allogenic human smooth muscle cells (SMCs) onto a biodegradable polymeric scaffold, followed by their long-term maturation in dynamic conditions. Eventually, the graft polymer degrades while concomitantly allowing the extracellular matrix (ECM) deposition from seeded cells. The developed graft was decellularized to prevent immune rejection, and these HAVs showed promising results in human clinical trials.[1,4,8d] One ostensible setback of acellular vascular grafts is their limited bioactivity, which is generally addressed by functionalizing them with specific bioactive molecules. The functionalization aims to prevent acute thrombosis and stenosis, allow faster endothelialization, and mitigate intimal hyperplasia. Notably, studies showing the immobilization of bioactive molecules onto polymeric vascular scaffolds focus on the singular aspect of graft remodeling. For example, heparin functionalization of poly(glycerol sebacate) (PGS) grafts helps in preventing thrombosis.[8a,9] Researchers have also demonstrated improved endothelialization of dimethyloxalylglycine (DMOG) functionalized polycaprolactone (PCL) grafts by enabling hypoxia mimicking response.[10] Vascular endothelial growth factor (VEGF) improves graft endothelialization by capturing the circulating progenitor cells and prevent acute thrombosis.[11] Other approaches include functionalization with integrin-binding ligand,[12] microRNAs,[13] nitric oxide (NO),[14] fibronectin,[15] CD133 antibody,[16] heparin,[11b,14] etc. Scaffold functionalization with a specific bioactive molecule improves the graft performance, but it is surmised not to mimic the efficacy of cell seeding. BMMNCs and other MSCs confer therapeutic efficiency by secreting important chemokines and cytokines, including immunomodulatory, angiogenic, and anti-apoptotic factors.[17] MSCs derived extracellular vesicles (EVs) hold a plethora of signaling molecules, including cytokines and microRNA.[18] Few recent studies have ventured into exploring EVs' incorporation in acellular polymeric grafts with great success.[19] Loading of EVs in PCL-based vascular grafts significantly improved their patency in the hyperlipidemic rat and mitigated calcification. Mechanistic analysis revealed the immunomodulatory ability of MSC-derived EVs, as they induced phenotype transition of macrophages from M1 pro-inflammatory to M2c anti-inflammatory type.[19a] MSC-derived exosomes also facilitated capturing endothelial progenitor cells (EPCs), assisting in faster endothelialization.[19b]

Among three potential sources of MSCs, bone marrow[3a,20] and adipose tissue-derived cells[21] have been widely explored in the field of vascular tissue engineering. By contrast, human Wharton's Jelly derived MSCs (WJMSCs) have shown limited application. Human Wharton's jelly ECM is a rich source of structural proteins (fibronectin, hyaluronic acid, collagens I, III, VI, XII, and tenascin-C)[22] and peptide growth factors (insulin-like growth factor 1 (IGF-I), platelet-derived growth factor (PDGF), fibroblast growth factor (FGF), transforming growth factor beta (TGF-β), epidermal growth factor (EGF), vascular endothelial growth factor (VEGF), tissue inhibitor of metalloproteinases 1 (TIMP1), etc.).[23] The matrix also contains the WJMSCs derived exosomes.[24] The human umbilical cord is a medical waste and could be made available in large quantities; hence, recent studies have ventured into investigating the Wharton's jelly (WJ) matrix for tissue engineering applications.[23b,25] The surface coating of glass coverslips with WJ matrix improved the growth and retention of vascular cells and MSCs.[23b] Interestingly, the secretome of WJMSCs has been reported to possess a higher amount of angiogenic factors than the secretomes derived from bone marrow (BMMSCs) and adipose-derived mesenchymal stem cells (ADMSCs).[26] Moreover, WJMSCs produce higher MCP-1 than their counterparts,[27] which is crucial for TEVG remodeling. WJMSCs secreted bioactive factors might facilitate in situ endothelialization, host cell recruitment, and constructive graft remodeling.[28]

Herein, aiming towards creating an acellular, clinically viable TEVG, silk-based vascular scaffolds are functionalized with decellularized human Wharton's Jelly (dWJ) matrix, for the first time. We hypothesized the preservation of WJMSCs secreted bioactive molecules in the WJ matrix, which might improve the performance of acellular TEVGs. In this work, we followed a modified protocol to obtain dWJ matrix from human umbilical cords, avoiding any harsh chemical (e.g., detergents) or enzyme treatment, which presumably prevents the loss of bioactivity of bioactive molecules in the matrix. Our previously reported bi-layered silk scaffolds are functionalized with dWJ matrix in this study, and in vivo graft performance is investigated in the rabbit jugular vein (JV) as an interposition grafting model.

2. Results

2.1. Decellularization and Cytokine Profile of Wharton's Jelly Matrix

The WJ matrix was obtained in the powdered form, post lyophilization, which was white in appearance and easily soluble in water without forming any clumps (**Figure 1**A). The aqueous solubility of dWJ matrix allowed it to mix with silk fibroin (SF) solution homogenously. A 5 mg of dWJ matrix was dissolved in 1 mL of silk solution (6% w/v) without showing any protein coagulation. However, on further increasing the dWJ concentration, silk protein coagulation was observed, resulting in lump formation. DNA quantification analysis revealed significantly less (10 times lesser) amount of DNA in dWJ matrix post decellularization ($\approx$40 ng mg^{-1} dry weight) as compared to native umbilical cord tissue ($\approx$400 ng mg^{-1} dry weight) ($p < 0.01$). In accordance

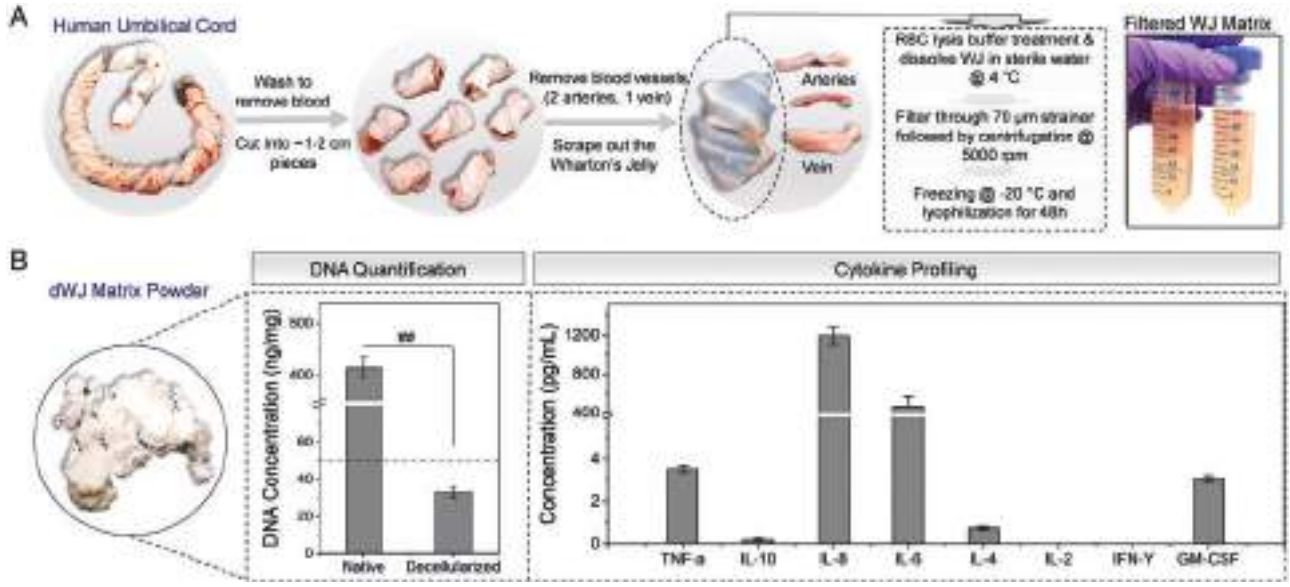

Figure 1. Isolation and characterization of human dWJ matrix. A) Scheme showing the stepwise process to isolate dWJ matrix. B) Aqueous dWJ solution was lyophilized to obtain powder form (white color) and re-dissolved in water to obtain the desired concentration. DNA quantification data are showing the decellularization of WJ matrix (n = 5). The dotted line represents the allowed threshold limit of DNA for decellularized tissue. Cytokine profiling of dWJ matrix showing the presence of immunomodulatory cytokines (n = 3). Data presented as mean ± SD, *p*-values are calculated using one-way ANOVA and post hoc Tukey's test, $\#\#p < 0.01$.

with a previous report, the DNA content of decellularized tissue was within the acceptable limit (50 ng mg^{-1} tissue).[29] We further analyzed the presence of inflammatory cytokines in dWJ matrix. Among the investigated cytokines, interleukin-8 (IL-8) concentration was maximum (1190 ± 94 pg mL^{-1}), followed by interleukin-6 (IL-6) (469 ± 100 pg mL^{-1}). Remaining cytokines were present in minimal amount: tumor necrosis factor alpha (TNF-α) (3.53 ± 0.13 pg mL^{-1}), granulocyte-macrophage colony-stimulating factor (GM-CSF) (3.09 ± 0.16 pg mL^{-1}), interleukin-4 (IL-4) (0.72 ± 0.08 pg mL^{-1}), and interleukin-10 (IL-10) (0.21 ± 0.04 pg mL^{-1}) (Figure 1B).

2.2. Human Decellularized Wharton's Jelly (dWJ) Treatment Improves Performance of Vascular Cells in Monolayer Culture

Live-cell imaging suggested that even at higher concentrations (1 mg mL^{-1}), dWJ matrix did not significantly affect the viability of both vascular cells (human umbilical vein endothelial cells (HUVEC) and human dermal fibroblasts (HDF)). Viable cells were observed after three days at all investigated concentrations, and no morphological alteration was observed compared to the standard tissue culture plate (**Figure 2**A,B and Figure S1A, Supporting Information). High magnification images of HUVEC are shown in Figure S2A, Supporting Information. Cell viability and proliferation were further quantified using the AlamarBlue assay. Cells proliferated ≈1.2-folds over three days in control and dWJ treated groups, signifying no detrimental effect of dWJ treatment on cell viability (Figure 2C and Figure S1B, Supporting Information). Subsequent increment of aqueous dWJ concentration adversely affected the HUVEC cell viability (Figure S2B, Supporting Information). Considering the biocompatibility of dWJ matrix with human endothelial cells up to 1mg mL^{-1}, we used the same concentration henceforth for further in vitro analysis.

The expression profile of various endothelial functional genes (Von Willebrand factor (vWF), cluster of differentiation 31 (CD31), endothelial nitric oxide synthase (eNOS), and vascular endothelial (VE)-Cadherin) by quantitative real-time PCR was investigated to assess the effect of dWJ matrix treatment onto cellular functionality. All of the studied genes play a crucial role in maintaining the overall blood vessel tone. Interestingly, endothelial cells showed significant upregulation of CD31 (≈2000-fold), eNOS (≈50-fold), and VE-cadherin (≈1600-fold) genes after dWJ matrix treatment ($p < 0.01$). However, vWF expression remained unchanged, and no significant difference was observed (Figure 2D–G).

After implantation in animals, graft remodeling relies on the recruitment and migration of host cells from the surrounding tissue. We performed the cell migration assay as an indirect measurement of cell migration from the host tissue to the graft. Results suggested a faster migration of HUVEC and HDF cells in the presence of dWJ matrix (observed at 30h) (Figure 2H,I and Figure S1C, Supporting Information). Quantification of the wound area corroborated a similar pattern. dWJ matrix treated group covered ≈85% wound area as compared to ≈40% for the untreated group ($p < 0.01$), signifying HUVEC migration at two times faster rate post dWJ treatment (Figure 2J). Similarly, around 2.5 times faster migration rate was recorded for HDF cells (Figure S1D, Supporting Information).

Furthermore, the amount of nitric oxide (NO) produced by endothelial cells was quantified, responsible for maintaining the vascular tone. At both time points (6 and 30h), endothelial cells treated with dWJ matrix produced a significantly higher (≈47 and ≈9 times, respectively) amount of NO than the control group

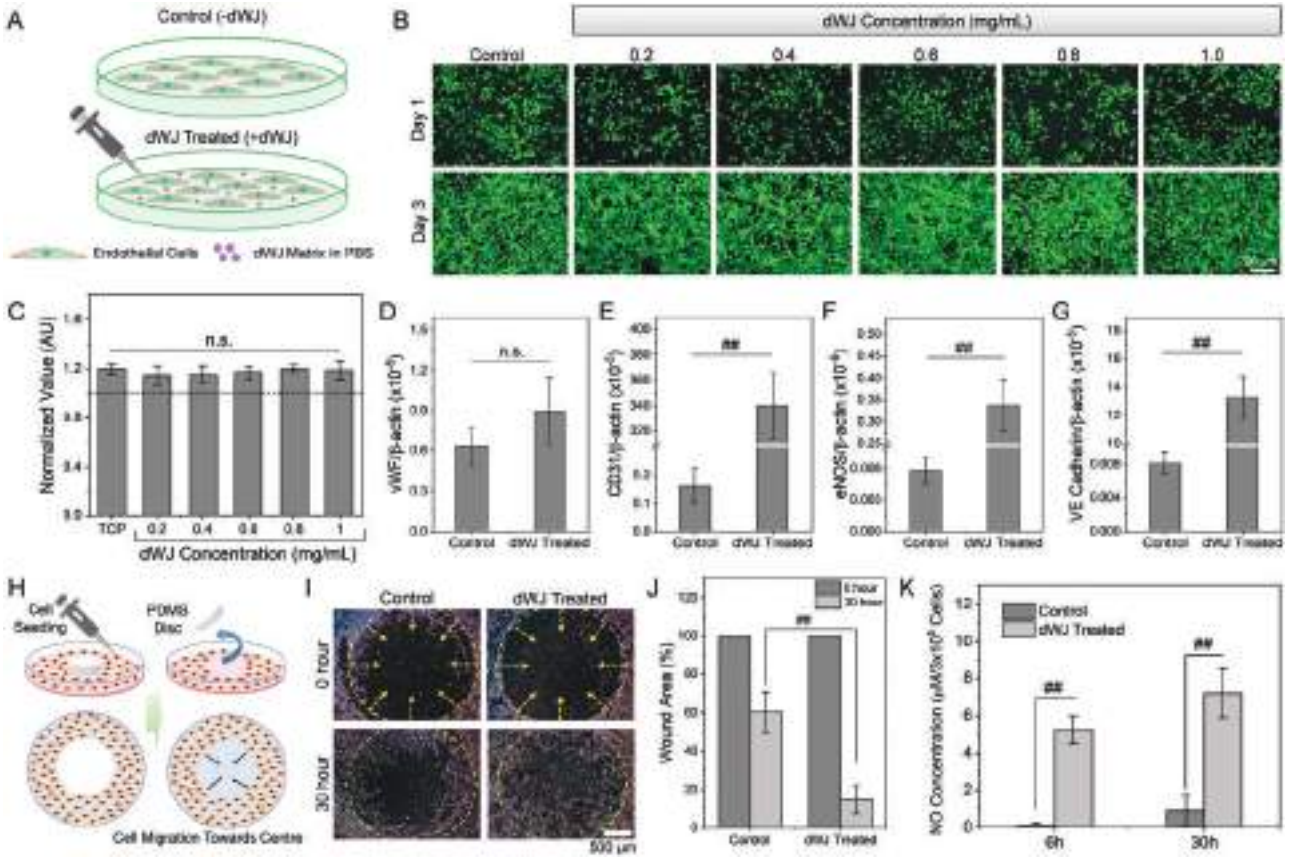

Figure 2. Effect of dWJ matrix on HUVECs viability and functionality. A) Schematic representation of aqueous dWJ matrix treatment on a 2D culture of HUVEC cells. B) Live-cell imaging showing the viability of HUVEC after 1 and 3 days of aqueous dWJ treatment at varying concentrations (0–1 mg mL^{-1}). C) Quantitative assessment of metabolic activity of HUVEC at different dWJ concentrations (n = 3). The dashed line is representing baseline metabolic cellular activity after one day of cell seeding. Real-time gene expression quantification for functional endothelial cell genes D) vWF, E) CD31, F) eNOS, and G) VE-Cadherin after 24h aqueous dWJ treatment (1 mg mL^{-1}) (n = 3). H) Scheme representing the process followed for analyzing the migration of HUVEC under the influence of aqueous dWJ treatment. I) Phase-contrast images of HUVEC processed using the "Find Edges" function of ImageJ, showing the migration of cells inwards towards the center of the circle marked with a yellow dashed line. Dotted arrows are representing the cellular migration towards the center. J) Quantification of cell migration in terms of percentage wound area over time (n = 4). K) Quantification of NO production from HUVEC after 6 and 30h aqueous dWJ treatment (n = 4). Data presented as mean ± SD, *p*-values are calculated using one-way ANOVA and post hoc Tukey's test, ##$p < 0.01$, n.s. = not significant.

($p < 0.01$) (Figure 2K). The NO concentration is reported after normalization with cell number.

2.3. Viability and Immunomodulation of Human THP-1 Monocytes Post dWJ Treatment

With recent advancements in the vascular tissue engineering field, it is now established that the circulating cells, including monocytes, play a crucial role in the maturation and remodeling of vascular grafts.[3a,11a] Hence, we investigated the effect of dWJ treatment on human monocytes (**Figure 3**A). The adherent THP-1 cells were subjected to various concentrations of dWJ matrix to analyze its cytotoxicity. MTT results showed no cytotoxic effect of dWJ matrix (0–1 mg mL^{-1}) on THP-1 derived macrophages (Figure 3B). The viability of the attached cells was further validated by live-dead fluorescence imaging. In both control and dWJ treated groups, mostly live cells (fluorescing green) were present with the negligible presence of dead cells (fluorescing red). The results indicated that dWJ matrix does not show any cytotoxic effects on THP-1 derived macrophages at 1 mg mL^{-1} concentration (Figure 3C).

Immunofluorescence imaging of control and dWJ treated THP-1 derived macrophages showed positive staining for cluster of differentiation 68 (CD68) and C-C chemokine receptor type 7 (CCR7). However, they markedly stained positive for cluster of differentiation 163 (CD163) in dWJ treated group (Figure 3D). These findings were further corroborated by image quantification analysis, wherein dWJ treated cells showed significantly higher CD163 expression as compared with the control group ($p < 0.01$) (Figure S3, Supporting Information). Quantitative real-time gene expression analysis revealed the downregulation of TNF-α, CCR7, and IL-6 genes, post 24h dWJ treatment. On the contrary, dWJ matrix induced the upregulation of MCP1, whereas no significant difference was observed for IL-10 (Figure 3E–I).

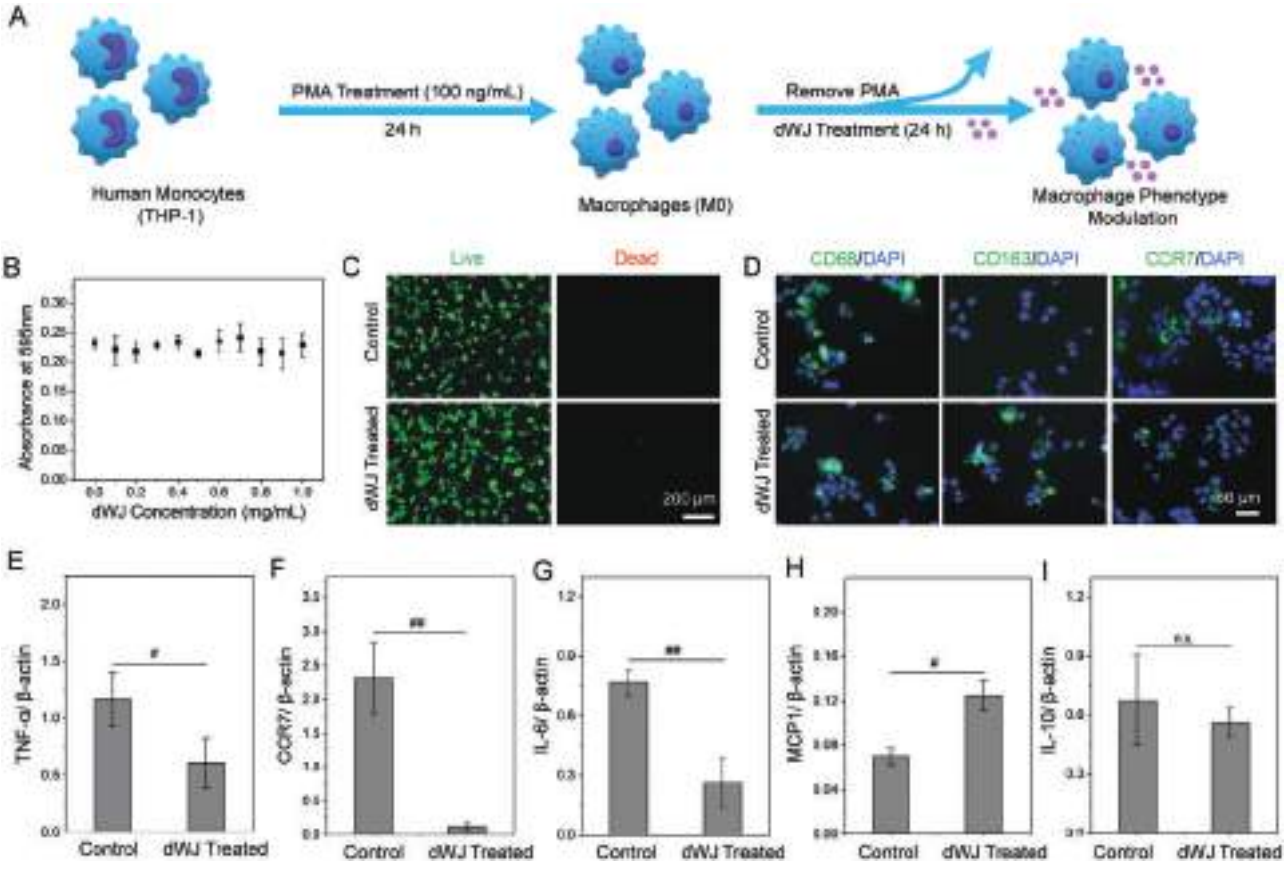

Figure 3. In vitro analysis of the effect of aqueous dWJ matrix treatment on human monocytes (THP-1). A) Scheme representing monocyte differentiation and aqueous dWJ treatment. B) Quantification of THP-1 cells viability after 24h dWJ matrix treatment (n = 4). C) Live/Dead fluorescent microscopic images showing the viability of THP-1 derived macrophages. D) Representative immunofluorescent images showing expression of CD68 (pan macrophage marker), CD163 (M2 marker), and CCR7 (M1 marker) in control and dWJ treated THP-1 derived macrophages. Real-time qPCR analysis quantifying the expression of E) TNF-α, F) CCR7, G) IL-6, H) MCP1, and I) IL-10 genes in control and dWJ treated THP-1 derived macrophages (n = 4). Data presented as mean ± SD, *p*-values are calculated using one-way ANOVA and post hoc Tukey's test, #$p < 0.05$, ##$p < 0.01$, n.s. = not significant.

2.4. Physical Characterization of Bi-Layered Tubular Silk Scaffolds and Assessment of Vascular Cell Viability and Migration

Bi-layered composite silk scaffolds were fabricated, as shown in **Figure 4**A. Three scaffold variants used in this study include: 1) BM (inner porous layer comprises *Bombyx mori* (BM) silk), 2) BA (inner porous layer comprises a combination of BM and *Antheraea assama* (AA) silk), and 3) BAW (BA functionalized with dWJ matrix). The porous core layer supports the recruitment and growth of host cells. The outer electrospun layer provides mechanical resilience to the graft and prevents the transmural flow of blood through the scaffold wall post-implantation. SEM images of grafts' cross-sections showed the inner porous and dense outer layer. None of the grafts revealed any delamination among the two layers (Figure S4, Supporting Information). The average thickness of the inner porous and the dense outer layer was 535 ± 38 and 51 ± 10 µm, respectively, resulting in 586 ± 48 µm total thickness of bi-layered scaffold wall. The core layer of all scaffold variants displayed the presence of interconnected pores (Figure 4B). Quantification of pore size of the core layer revealed an overlapping distribution ranging 20–65 µm (mean value of 40µm) for BM, 20–72 µm (mean value of 40 µm) for BA, and 10–55 µm (mean value of 32 µm) for BAW scaffolds ($p > 0.05$) (Figure 4C). A minor, insignificant shift in porosity range for BAW scaffolds might be resulting from the presence of structural components of WJ matrix.

In vitro scaffold degradation data revealed a faster degradation in the presence of protease enzyme for all variants ($p < 0.01$). In both treated and untreated groups, BAW scaffolds showed a comparatively faster degradation profile than BM and BA scaffolds. Minimal scaffold degradation (10.43 ± 1.58% and 7.70 ± 4.87% mass loss for BM and BA scaffolds, respectively, over 28 days) was recorded in the absence of enzyme; however, BAW scaffolds showed significantly higher mass loss (30.33 ± 5.94%) ($p < 0.01$). A similar trend was observed for the enzyme-treated group over 28 days (50.68 ± 9.28% and 55.05 ± 2.96% vs 77.78 ± 10.92% for BM and BA vs BAW, respectively) ($p < 0.01$) (Figure 4D). Further analysis of scaffold swelling property (water retention ability) revealed a superior swelling ratio for BAW scaffolds (12.25 ± 0.6) as compared with BM and BA scaffolds (10.01 ± 0.52 and 9.88 ± 0.5 respectively) post 300 mins ($p < 0.01$). Early swelling data showed that all scaffold variants reached saturation after 30 min and followed the same trend at later time points (Figure 4E). To analyze the scaffold integrity

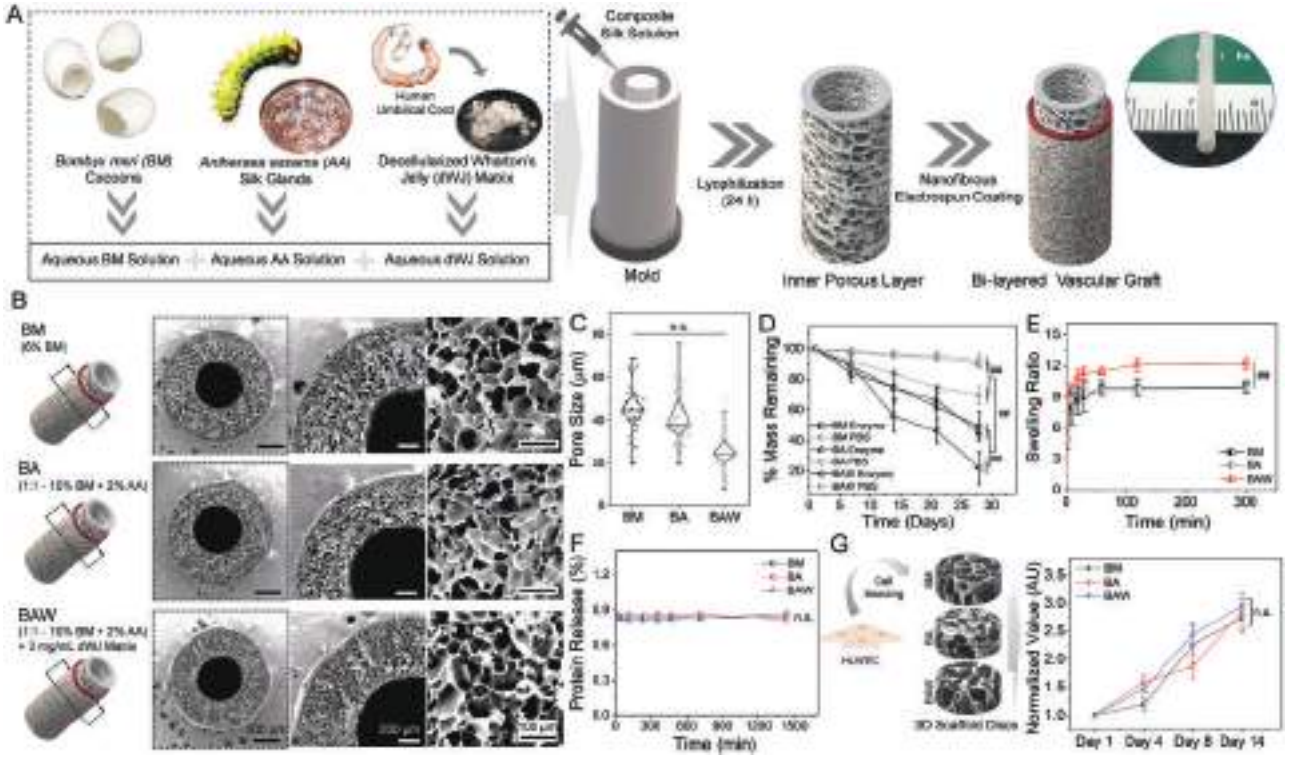

Figure 4. Fabrication and physical characterization of tubular silk bi-layered vascular grafts and HUVEC growth profile. A) Representative scheme showing the stepwise fabrication of bi-layered silk vascular grafts. B) Scanning electron microscopic (SEM) images of grafts' cross-sections show porosity and pore interconnectivity of the inner core layer. C) Graph representing quantification of pore size of the inner porous layer for all three scaffold variants calculated by processing the SEM images (n = 6, each group). D) In vitro quantification of scaffold degradation in control (PBS) and treated (protease enzyme) groups over 28 days (n = 6). E) Graph representing water retention capability of silk scaffolds (n = 6). F) Quantification of protein release from silk scaffolds (n = 6). G) Schematic representation on the left shows seeding of HUVEC onto 3D porous silk scaffolds discs (BM, BA, and BAW). The graph on the right represents a quantitative measurement of HUVEC proliferation onto 3D silk scaffolds over 14 days (in terms of the normalized metabolic activity assessed through AlamarBlue assay) (n = 4). Data presented as mean ± SD, *p*-values are calculated using one-way ANOVA and post hoc Tukey's test, #$p < 0.05$, ##$p < 0.01$, n.s. = not significant.

and ensure stable crosslinking, protein release from scaffolds was quantified for 24h. Results suggested less than 1% protein release for all scaffold variants corroborating their stability (Figure 4F). An extended time-point water retention and protein release profiles showed a similar trend up to 28 days (Figure S5, Supporting Information). BAW scaffolds at the pre-implantation stage showed positive staining for collagen I (col-I), corroborating the stable integration of dWJ matrix components in the scaffold struts (Figure S6, Supporting Information). High magnification SEM images revealed a smoother surface of BM and BA scaffold struts; whereas, a significantly rougher surface for BAW. Notably, cross-sections of scaffold struts showed fibrous structures, substantiating the presence of dWJ matrix structural components in BAW scaffolds (Figure S7, Supporting Information).

The proliferation of endothelial cells on 3D BM, BA, and BAW scaffolds was analyzed by measuring the metabolic activity over 14 days. The result is reported after normalization with day one values (Figure 4G). All three scaffold types supported the endothelial cell growth over 14 days, and no significant difference was observed in the growth rate among experimental groups. On day 14, a ≈threefold increase in cell number was recorded compared with day 1. The results suggest that in 3D porous silk scaffolds, the presence of dWJ matrix in BAW did not significantly affect the growth rate of endothelial cells. HDF migration analysis in 3D porous silk scaffolds revealed significant improvement in cell migration rate in BAW scaffolds on day 7, calculated in terms of % area coverage over time (Figure S8, Supporting Information).

2.5. Macrophage Response and Immunomodulation Ability of dWJ Functionalized 3D Silk Scaffolds Implanted in Rabbit Subcutaneous Pocket

As shown in **Figure 5**A, 3D silk scaffold discs were implanted in the subcutaneous pocket of rabbits followed by sample retrieval at five days and one month, post implantation. Qualitative assessment of hematoxylin & eosin (H&E) stained images showed a higher cellular infiltration at early point (five days) than one-month explants, signifying the host's initial inflammatory response followed by eventual graft acceptance. Interestingly, more cells were recruited by dWJ functionalized scaffolds (BAW) than other experimental groups after five days. In addition, cells were arranged along the scaffold struts suggesting their superior bioactivity (Figure 5B). Immunostaining of infiltrated cells showed positive staining for CD68, a pan macrophage marker,

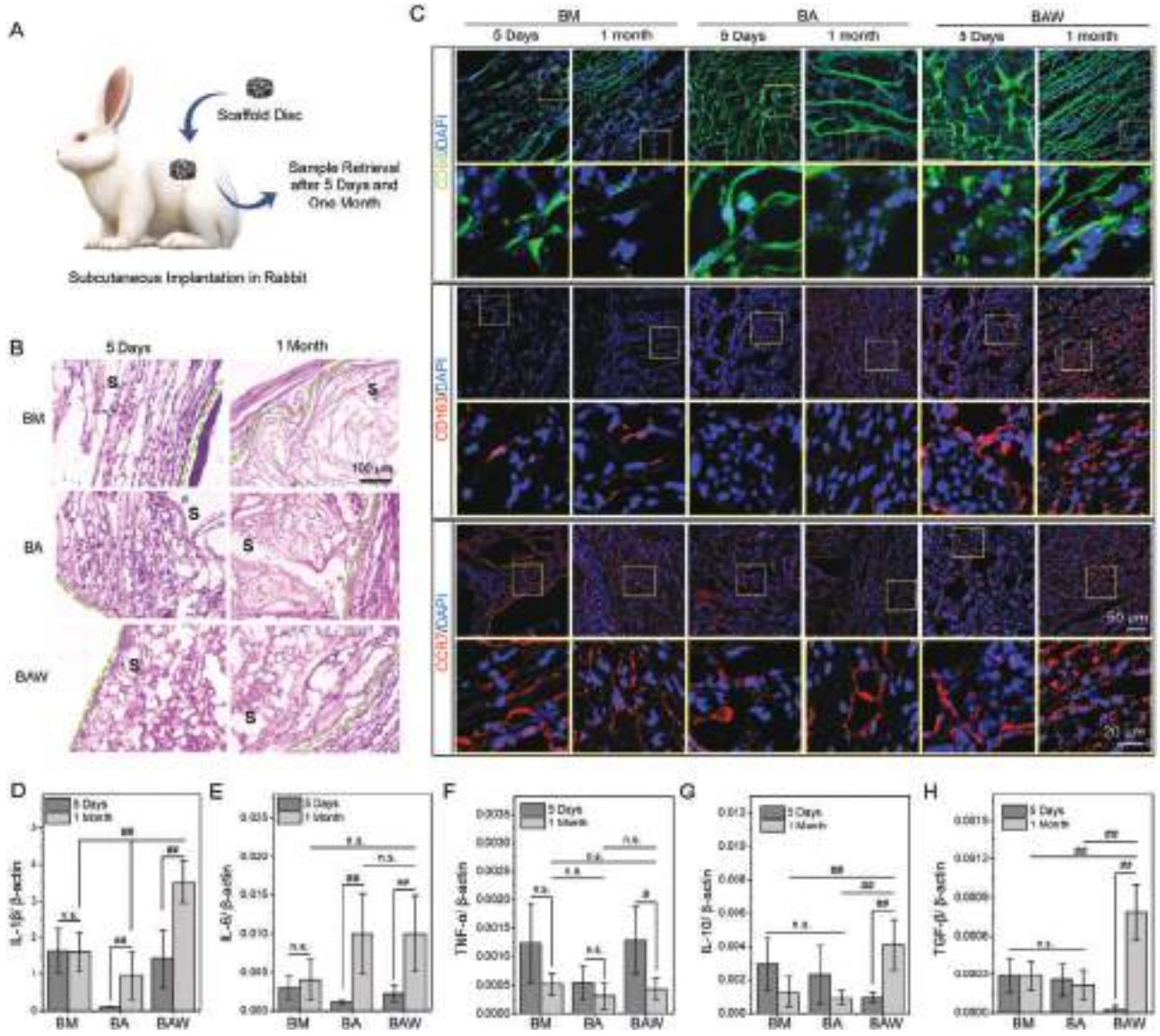

Figure 5. In vivo immunomodulation analysis of dWJ functionalized silk scaffold discs in rabbit subcutaneous implantation model. A) Schematic representation of subcutaneous implantation of silk/dWJ scaffolds in rabbits, followed by retrieval after five days and one month. B) Hematoxylin & eosin (H&E) stained histology sections of silk scaffold explants. The scaffold is marked as "s", and dotted green lines are representing the host tissue-scaffold interface. C) Immunofluorescence staining of explanted silk scaffolds sections for CD68 (pan macrophage marker), CD163 (M2 macrophage marker), and CCR7 (M1 macrophage marker). For each specific antibody, the bottom row is the magnified image of the square labeled portion of the top row. D–H) Quantification of real-time gene expression of M1 (IL-1β, IL-6, and TNF-α) and M2 (IL-10 and TGF-β) phenotypic markers in five days and one month explants of silk scaffolds (n = 3). Data presented as mean ± SD, p-values are calculated using one-way ANOVA and post hoc Tukey's test, #$p < 0.05$, ##$p < 0.01$, n.s. = not significant.

corroborating macrophage recruitment in all scaffold types following five days of implantation. In agreement with histological data, considerably higher $CD68^+$ cells were observed in 1-month BAW explants. A similar trend was observed for $CD163^+$ cells (representing M2 anti-inflammatory phenotype). In contrast, all scaffolds showed a homogenous presence of $CCR7^+$ cells (representing M1 pro-inflammatory phenotype) at both time points (five days and one month) (Figure 5C).

Quantitative expression of M1 (IL-1β, IL-6, and TNF-α) and M2 (IL-10 and TGF-β) phenotype-specific genes was further studied to analyze the impact of dWJ functionalization on macrophage polarization. Resident macrophages in BM scaffolds showed comparable expression of all genes at both time points. BA scaffolds showed an elevated level of pro-inflammatory genes after one month compared with five days ($p < 0.05$), except for TNF-α, where no significant difference was observed among both the time points. Similarly, comparable expression of anti-inflammatory genes was evidenced at different time points for BA scaffolds. Interestingly, BAW scaffolds showed immunomodulatory activity. Upregulation of pro-inflammatory genes was

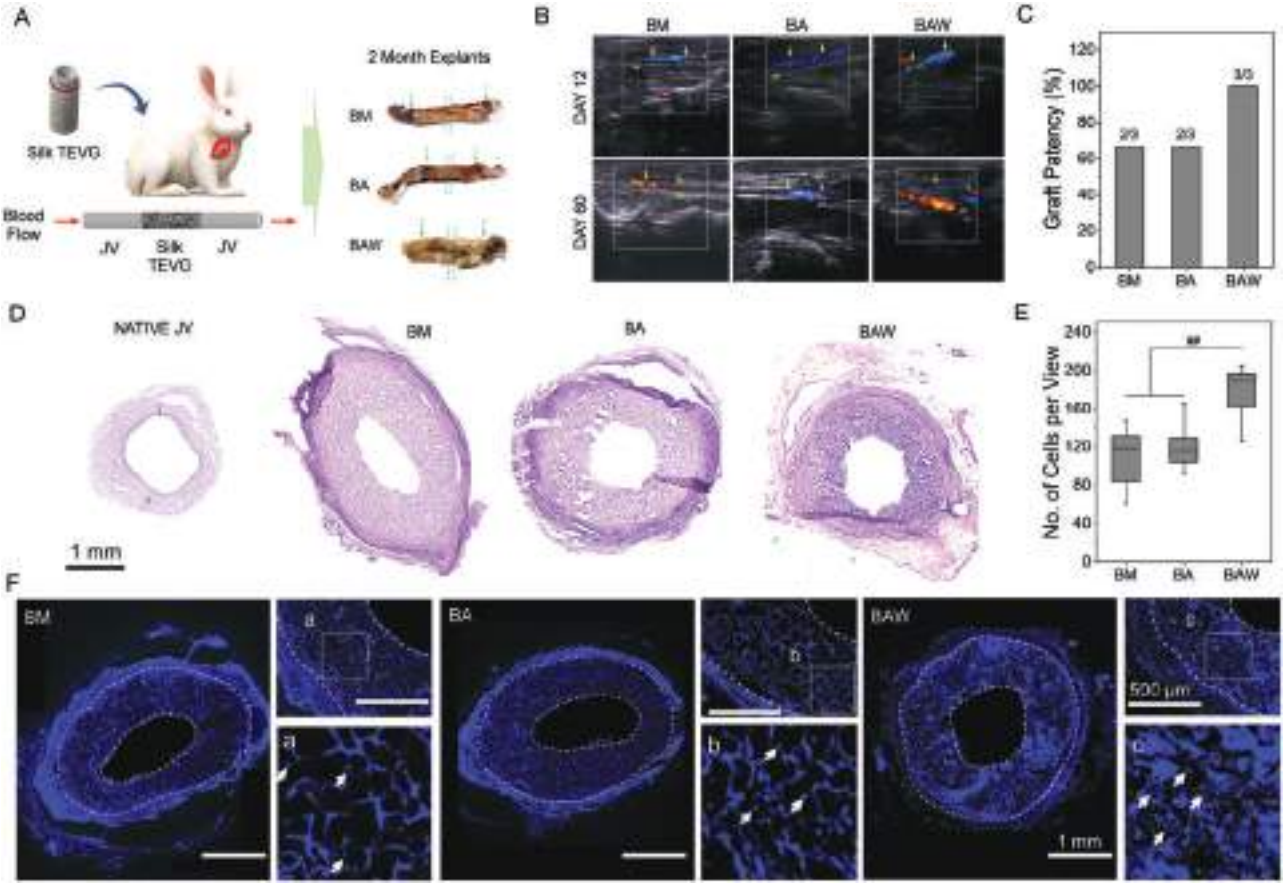

Figure 6. In vivo implantation of silk TEVGs in rabbit JV. A) Schematic representation of interposition grafting of silk TEVGs in rabbit JV (n = 3 for each experimental group). Grafts were explanted after two months. Dotted arrows are indicating the anastomotic point between TEVG and JV. Dotted lines in the middle portion of the graft represent the section used for histological analysis. B) Representative color Doppler imaging of implanted TEVGs after 12 days and 60 days of implantation. Yellow arrows are representing the anastomotic site. C) Patency analysis of silk TEVGs based on color Doppler data. D) H&E stained histological cross-sections of native JV and silk explants, demonstrating host cell infiltration into silk TEVGs. E) Quantification of host cells infiltrated into silk TEVGs (n = 6 images processed per experimental group). F) DAPI stained fluorescent microscopic images of silk TEVG explants' cross-sections staining cell nucleus blue. White arrows are representing the presence of cell nuclei in each section. The square portions having white outlines labeled as a, b, c are further magnified in the bottom images. *p*-values are calculated using one-way ANOVA and post hoc Tukey's test, $\#\#p < 0.01$.

observed over time (from day 5 to 1-month) ($p < 0.01$), except for TNF-α, which was downregulated after one month ($p < 0.05$). In addition, significant upregulation of anti-inflammatory genes was recorded for one month BAW scaffold explants ($p < 0.01$). IL-10 and TGF-β expression for BAW explants was significantly higher than other scaffold variants at one month (Figure 5D–H).

2.6. Patency Analysis and Host Cell Infiltration in Silk TEVGs

Silk TEVGs were implanted in rabbit JV as interposition grafts by an end-to-end anastomosis (Figure S9A, Supporting Information). The bi-layered silk scaffolds were easy to handle during the microsurgical procedure and withstood the intraluminal venous blood pressure without any sign of leakage. After removing surgical micro-clips, faint graft-reddening was observed, ensuring the recirculation of blood flow through the graft. After two months, the grafts were explanted, and an overall gross morphological overview suggested a resolved fibrotic response. Compared to BM and BA explants, BAW explant showed thicker fibrous capsule formation over the graft representing inflammatory response (Figure S9B, Supporting Information). Neo-tissue formation and the presence of microvessels over the graft surface indicate their integration with the native tissue. It was also corroborated by investigating the anastomotic graft site showing graft-native tissue (JV) integration (**Figure 6**A). Graft patency was confirmed by color Doppler imaging after 12 and 60 days of implantation. After 12 days of implantation, none of the grafts showed any sign of occlusion, precluding the possibility of acute thrombosis. However, color Doppler images of one of each BM and BA grafts after 60 days of implantation showed occlusion (Figure 6B). H&E stained histological sections of occluded silk TEVG explants suggested the cellular overgrowth in the lumen (Figure S10, Supporting Information). The overall graft patency was 66.66% (2/3) for BM and BA grafts, whereas BAW grafts showed 100% patency (3/3) after two months without any sign of lumen narrowing (Figure 6C).

The explanted silk scaffolds were further analyzed by investigating the histology cross-sections. H&E stained images of explants and native rabbit JV are shown in Figure 6D. High magnification images of silk TEVG scaffolds before implantation (negative control) and after two months of implantation in rabbit JV are shown in Figure S11, Supporting Information. While no cells were present in the negative control, significant infiltration of host cells was observed in two month explants of all silk TEVGs. Histological images of patent grafts suggested that the lumen diameter of silk explants was similar to the native JV (Figure S12, Supporting Information). Histological images revealed neo-tissue formation at luminal and ablumen surfaces covering the scaffold wall. Most of the scaffold struts were evident for BM and BA grafts; however, the cross-section of BAW explant exhibited comparatively lesser scaffold struts. The latter observation indicates the possibility of a higher degree of graft remodeling over time for BAW grafts compared with other counterparts (BM and BA), which might be co-related with graft degradation rate suggesting a faster degradation rate of BAW grafts facilitating rapid neo-tissue formation.[8a] We further investigated the host cell infiltration in the silk grafts, which revealed approximately 1.6-fold higher cells in BAW grafts than BM/BA grafts. Homogenous distribution of cells was observed in the scaffold walls radially (Figure 6E,F). Fluorescence microscopic images of bare silk TEVGs are shown in Figure S13, Supporting Information, representing the autofluorescence of scaffolds.

2.7. In Vivo Remodeling of Silk TEVGs

Remodeling of explanted silk TEVGs was monitored by qualitative and quantitative assessment of remodeled tissue. The immunohistological analysis for CD31 suggested homogenous endothelialization of BAW grafts along the lumen; however, BM and BA grafts demonstrated discontinuation of the endothelium (**Figure 7**A). A quantitative analysis of % area covered by $CD31^+$ cells revealed significantly higher endothelialization in BAW explants (Figure 7B). SMCs in the developed neo-tissue were further substantiated by positive staining for αSMA and calponin (early and mid differentiation markers for SMCs). The qualitative assessment suggested densely packed SMCs in the scaffold wall for BA and BAW, whereas BM grafts showed a comparatively lesser density of SMC population. Overall, this data suggests that BAW grafts developed a superior neo-tissue comprising luminal endothelial cells (ECs) and medial SMCs over the experimental period than BM/BA grafts. BA grafts, although showed a predominant presence of SMCs in contrast with BM grafts, yet both BM and BA grafts performed poorly in terms of endothelialization as compared to BAW grafts (Figure 7A).

Two month silk explants were further analyzed for graft remodeling and ECM (collagen and elastin) deposition. In corroboration with DAPI staining data, H&E stained sections revealed the elevated host-cell infiltration in BAW scaffolds. The elastin content of the explants was stained by Verhoeff Van Gieson (VVG) staining, which revealed minimum elastin in BM scaffolds. On the other hand, a dense deposition of unorganized elastin was observed for BA and BAW grafts. On a similar note, collagen deposition followed a similar pattern as that of elastin with maximum collagen content present in BAW grafts, as revealed by Masson's trichrome (MT) staining of graft cross-section (Figure 7A). We also looked into any calcification in the silk graft by staining the explant sections with alizarin red dye. The results revealed that the silk grafts and the native rabbit JV were devoid of any calcium content (Figure S14, Supporting Information).

ECM quantification data suggested an elevated presence of collagen and elastin in two months BAW explants compared to other experimental groups. The amount of collagen was comparable for the native JV, BA, and BAW ($p = 0.057$ for both); however, BM explants showed significantly lower collagen content than the JV ($p = 0.013$). No significant difference was observed among silk explants ($p > 0.05$) (Figure 7C). Elastin quantification showed significantly lower levels in two months silk explants than native JV (approximately 20%, 24%, and 36% for BM, BA, and BAW explants) ($p < 0.01$). The elastin content for BAW explants was higher than BA ($p < 0.05$), and BM ($p < 0.01$) explants (Figure 7D).

For mechanistic analysis of graft remodeling post-implantation, histological sections were immunostained to mark the presence of tissue-resident macrophages as well as their phenotypes as a result of the inflammatory response (**Figure 8**A). Quantification of % area revealed a high population of $CD68^+$ cells in BAW ($11.68 \pm 1.58\%$) than BM and BA grafts ($5.54 \pm 0.74\%$ and $7.36 \pm 0.71\%$, respectively) ($p < 0.05$), signifying increment of approximate twofold than BM and 1.6-fold than BA grafts (Figure 8B). A similar trend was observed for M2 anti-inflammatory macrophage marker CD163, for which % area coverage was 5.95 ± 0.51 for BAW versus 2.68 ± 0.4 and 4.38 ± 0.59 for BM ($p < 0.01$) and BA grafts ($p < 0.05$) respectively (Figure 8C). On the contrary, BA ($5.76 \pm 0.83\%$) and BAW grafts ($6.34 \pm 1.09\%$) showed a comparable population of $CCR7^+$ cells (M1 pro-inflammatory marker) ($p > 0.05$), which were significantly higher than BM grafts ($3.42 \pm 0.38\%$) ($p < 0.05$) (Figure 8D). To assess the anti-inflammatory immunomodulatory behavior of dWJ functionalized silk grafts, the ratio of $CD163^+/CCR7^+$ was calculated. A significantly higher ratio for BAW grafts (0.96 ± 0.18) attested to the presence of comparatively higher M2 macrophages density, possibly improving pro-remodeling effects in BAW graft than other silk graft variants (Figure 8E).

2.8. Biomechanical Characterization of TEVG Explants

Uniaxial circumferential tensile testing data were obtained using tissue explant rings, as shown in **Figure 9**A. Stress-strain curves of BM and BA samples revealed a more linear pattern, which is representative of materials. On the other hand, BAW explants showed an exponential response (a J-shaped curve), a characteristic feature of soft biological tissues (Figure 9B–D). In the toe region, no significant modulus difference was recorded among silk TEVG explants; however, BAW explants revealed maximum linear modulus (0.68 ± 0.38 MPa), significantly higher than BM (0.18 ± 0.02 MPa, $p = 0.07$) and BA (0.22 ± 0.07 MPa, $p = 0.09$) counterparts (Figure 9E,F). Further exploration of stress values at failure point revealed a similar pattern, wherein BAW samples showed maximum stress (0.81 ± 0.23 MPa), significantly higher than BM (0.23 ± 0.03 MPa) and BA (0.36 ± 0.07 MPa) explants ($p < 0.01$) (Figure 9G). The corresponding strain was comparable

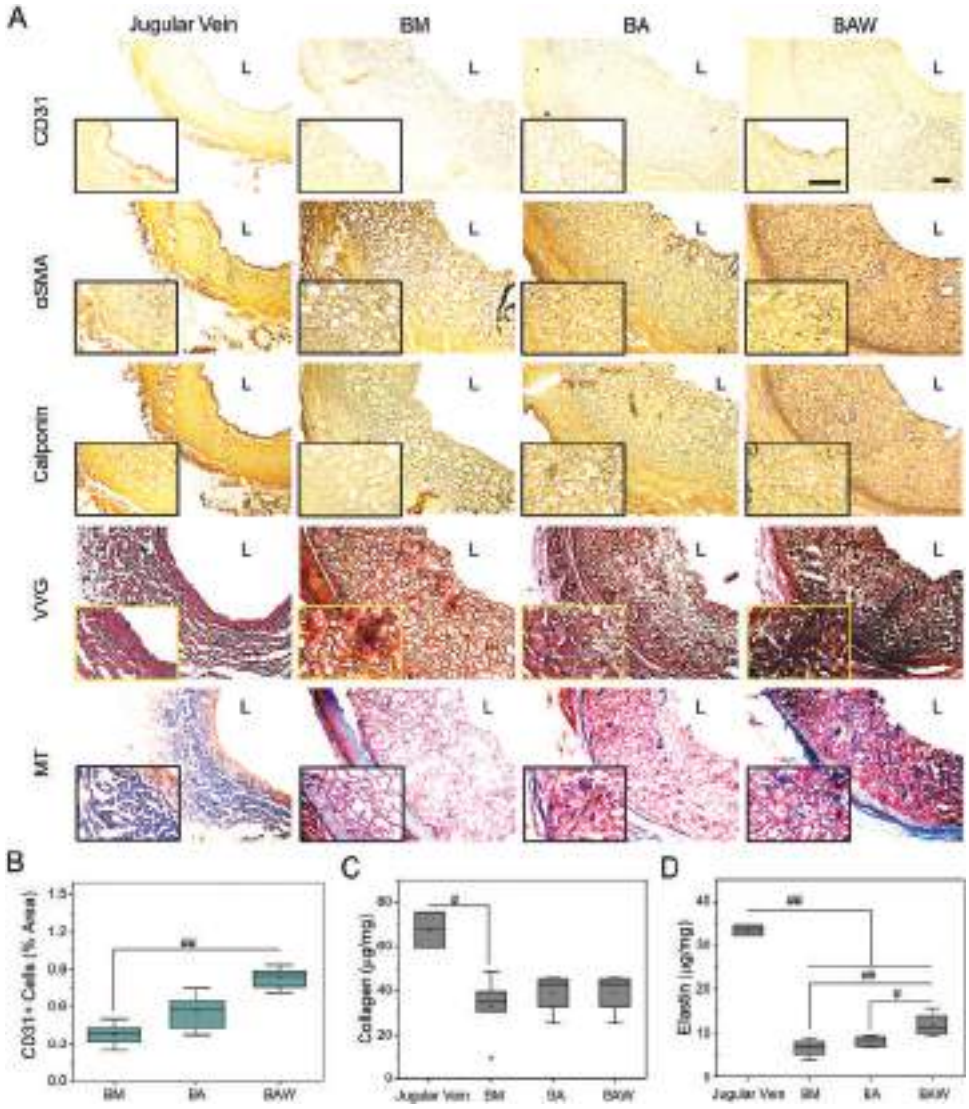

Figure 7. Analysis of silk TEVG remodeling after two months implantation in rabbit JV as interposition graft. A) Representative immunostained histological images of native rabbit JV and silk TEVG explants showing the presence of vascular cells (CD31: endothelial cell marker, calponin, and αSMA: SMCs marker at early and mid-differentiation phase respectively) in the remodeled grafts. Representative histological images of silk TEVG explants and rabbit JV showing ECM deposition (VVG for Elastin: blue-black to black color and MT for Collagen: blue color). Inset images are showing the magnified zone of interest for each specific stain. Lumen is marked as "L". Scale bar: 100 μm. B) Graph representing quantification of percentage area covered by CD31+ cells (representing endothelial cells) in histological cross-sections of silk TEVG explants (n = 6 images per experimental group). Quantification of C) collagen and D) elastin, in remodeled silk grafts compared with the native JV (n = 3). *p*-values are calculated using one-way ANOVA and post hoc Tukey's test, #$p < 0.05$, ##$p < 0.01$.

for all samples ($p > 0.05$) (Figure 9H). Circumferential biomechanical properties of BAW silk explants were similar to either native human saphenous vein (hSV) or porcine internal mammary artery (pIMA) (**Table 1**).

3. Discussion

Research impetus in the field of vascular tissue engineering is lately witnessing a lateral shift towards cell-free grafts. The goal is to reduce the clinical testing time and make the grafts readily available for patients in need. Cell-free polymeric grafts can be manufactured in large quantities with high fidelity circumventing the limitations of auto/allografts; however, their blood compatibility and remodeling ability remain questionable. Previously, we have shown the remodeling ability of stromal vascular fraction (SVF) seeded bi-layered silk scaffolds.[21] Albeit, it is believed that acellular grafts would have better chances to enter into the clinic. With the latest advancements, studies have revealed that cell-seeding, be it either vascular cells or various MSCs, is not as vital for graft viability (in terms of patency, endothelialization, and remodeling). Acellular grafts functionalized with different bioactive molecules have shown comparable in vivo performance.[2,8a] There is now enough scientific evidence that MSC seeded grafts remodel via paracrine fashion. Among

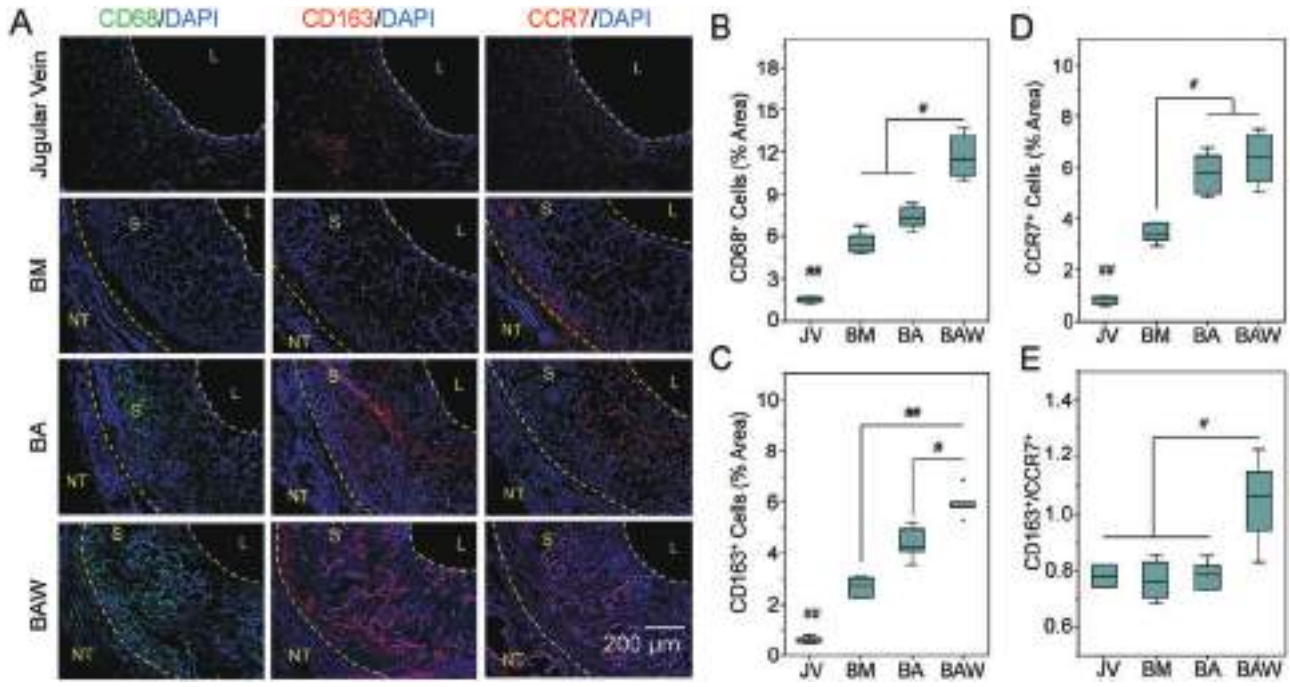

Figure 8. Macrophages and their phenotype in silk TEVG explants. A) Immunofluorescent histological images of vascular silk explants showing the presence of $CD68^+$ (pan macrophage marker), $CD163^+$ (anti-inflammatory marker), and $CCR7^+$ (pro-inflammatory marker) cells. L = Lumen, S = Scaffold, NT = Neotissue). Quantification of percent area of B) CD68, C) CD163, and D) CCR7 markers obtained by processing the immunofluorescent images (n = 6 for each experimental group) using ImageJ. E) Graph representing M2/M1 marker positive cells. *p*-values are calculated using one-way ANOVA and post hoc Tukey's test, $\#p < 0.05$, $\#\#p < 0.01$.

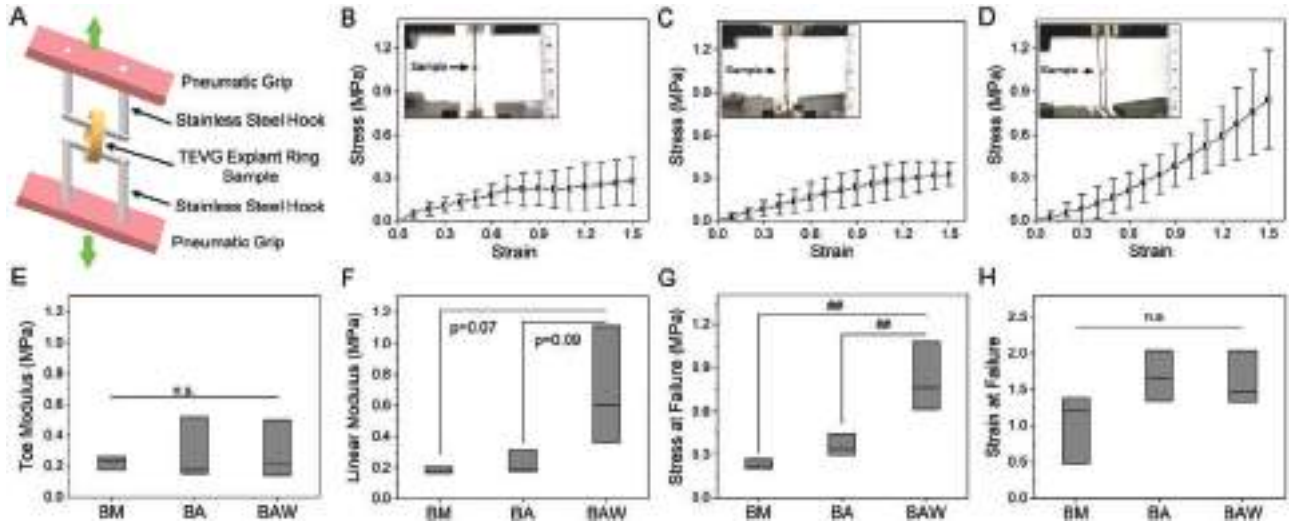

Figure 9. Biomechanical assessment of silk TEVG explants. A) Schematic representation of uniaxial circumferential tensile testing set-up. The tissue rings (n = 3 for each experimental group) were mounted in stainless steel hooks through the lumen. Hooks were pulled apart at 2 mm min^{-1} crosshead speed until sample failure. Average representative stress-strain curves for B) BM, C) BA, and D) BAW TEVG explants. Graphs are representing modulus in E) low stretch (toe modulus) and F) high stretch (linear modulus) regions. G) Maximum stress and H) corresponding strain at failure points. *p*-values are calculated using one-way ANOVA and post hoc Tukey's test, $\#\#p < 0.01$, n.s. = not significant.

numerous soluble factors, MCP-1 has been identified to be playing a significant role in graft remodeling.[3a] Other strategies towards successful grafting involve approaches for faster endothelialization to prevent acute thrombosis. The current rationally important requisite is to biologically functionalize the acellular polymeric grafts, which can prevent acute thrombosis, induce endothelialization, and help in constructive graft remodeling. The goal of the present study was to identify a novel cell-free solution for tissue-engineered polymeric vascular grafts aiming to expedite their clinical translation. Herein, as a potential alternative

Table 1. Biomechanical circumferential tensile properties of silk explants compared with previously reported hSV and pIMA.

	BM	BA	BAW	Human saphenous vein (hSV)[30]	Porcine internal mammary artery (pIMA)[30]
Stress at failure [MPa]	0.23 ± 0.03	0.36 ± 0.07	0.81 ± 0.23	3.7 ± 2.0	10.4 ± 7.1
Strain at failure	1.02 ± 0.48	1.67 ± 0.34	1.61 ± 0.37	1.7 ± 0.7	1.5 ± 0.2
Modulus [MPa]	Toe: 0.22 ± 0.04	Toe: 0.28 ± 0.20	Toe: 0.28 ± 0.18	2.5 ± 1.0	0.4 ± 0.2
	Linear: 0.18 ± 0.02	Linear: 0.22 ± 0.07	Linear: 0.68 ± 0.38		

for cell seeding, we propose the functionalization of cell-free silk TEVGs with dWJ matrix. The dWJ matrix obtained by a facile modified approach is hypothesized to prevent the loss of bioactivity of in-house extracellular components due to the following reasons: 1) tissue is processed at 4 °C, and 2) it avoids the use of detergents and enzymes. Considering the superior performance of BA grafts in our earlier work,[21] herein we functionalized them with dWJ matrix (referred to as BAW). The dWJ functionalization was aimed to support endothelialization and allow constructive remodeling after implantation, considering the intrinsic presence of angiogenic and immunomodulatory factors. We surmised that our dWJ functionalized TEVGs possess the benefit of WJMSCs' bioactivity. In addition, BM silk TEVGs were investigated as a silk control group in accordance with our previous study.[21]

Recruitment of host cells in the acellular polymer graft post-implantation is the starting point for their remodeling. The implanted TEVG is populated by host cells by either one of the following processes: trans-anastomotic, fall-out, and transmural migration.[2] Instantly after TEVG implantation, the scaffold wall is infused with blood, facilitating the infiltration of vascular progenitor cells and circulating monocytes via the fall-out process. These cells are envisioned to populate the graft in an acute response, in addition to the host inflammatory immune response. The sparse availability of circulatory vascular progenitor cells strengthens the idea that a vast majority of early phase infiltrated cells comprise circulatory monocytes. In addition, as a part of the host immune response, tissue-resident monocytes infiltrate the wound site and differentiate into macrophages. The recruited macrophages initially exhibit a pro-inflammatory (M1) phenotype known to stimulate angiogenesis, followed by a transition into a diverse anti-inflammatory (M2) population consisting of various subtypes participating in tissue remodeling.[31] Macrophage plasticity is effectively involved in TEVG remodeling, which is regulated by specific cytokines and other factors. Cytokine profiling of dWJ matrix revealed the presence of following immunomodulatory factors: IL-8, IL-6, IL-10, IL-4, TNF-α, and GMCSF. Previous reports suggest that IFN-γ and TNF-α stimulate the M1 phenotype of macrophages. In addition, various subtypes of M2 phenotypes are stimulated by selective cytokines.[32] For instance, IL-4, IL-10, and IL-6 are reported to induce M2 phenotype (pro healing and pro remodeling).[32] M2 phenotype also promotes the secretion of matrix metalloproteinases (MMPs), leading to tissue remodeling. Other cytokines like IL-8 are associated with neutrophil recruitment, the first inflammatory cell to reach the injury site. Prior studies suggest that M2 macrophages induce tissue remodeling by manipulating fibrosis and ECM deposition.[32] Notably, we observed significantly high recruitment of macrophage population in a 5-day subcutaneous explant of the BAW scaffold (Figure 5B), possibly either due to the upregulation of MCP1 gene in the resident macrophages (Figure 3H) or intrinsic presence of MCP1 protein in dWJ matrix.[27] However, a detailed proteomic analysis is needed to ascertain the presence of MCP1 protein in dWJ matrix.

Considering the plasticity of macrophage phenotypes and the presence of immunomodulatory factors in dWJ matrix, we further delved into determining the fate of recruited macrophages. Short-term in vitro dWJ exposure to human macrophages (THP-1) downregulated M1-associated genes (TNF-α, CCR7, and IL-6) but did not affect the IL-10 expression. However, immunofluorescence images indicated CD163 expressing cells (representing M2 macrophages), suggesting a possible switch towards the M2 phenotype. Further long-term in vivo rabbit subcutaneous implantation study validated the former observation, and significantly higher $CD163^+$ cells were traced in BAW explants. Although, CCR7 expression was evident in all experimental groups (Figure 5C). Interestingly, quantification analysis revealed the upregulation of M2 markers (IL-10 and TGF-β) in BAW scaffolds over time, whereas M1 markers (IL-1β, IL-6, and TNF-α) showed an ambiguous response. Overall, this data represents that dWJ functionalization of silk TEVGs should favor M2 anti-inflammatory macrophage phenotype and promote graft remodeling, which was corroborated by a significantly higher M2/M1 ratio for BAW TEVG explants, validating the role of dWJ functionalization in expediting the tissue remodeling (Figure 8E).

Another indispensable pre-requisite for functional remodeling of the implanted TEVG is the formation of neo-tissue comprising of vascular cells (endothelial cells, SMCs, and fibroblasts). Vascular cells from the adjacent native tissue are believed to populate the implanted TEVG via transanastomotic and transmural migration. Herein, we observed that dWJ matrix treatment accelerated the in vitro migration rate of endothelial and fibroblast cells (Figure 2J, Figure S1D and S8, Supporting Information), which spurs the notion that bio-composite silk vascular grafts may demonstrate faster remodeling. Silk TEVG 2 month explants from rabbit JV substantiated our in vitro findings as represented by higher cell infiltration in BAW explants than control groups (BM and BA) (Figure 6E). The role of the RGD cell-binding motif in AA silk should also be acknowledged.[21] TEVGs modified with RGD tripeptide showed 3-times higher endothelial coverage in rabbit carotid artery post four weeks. These grafts also recruited significantly more SMCs and showed superior patency compared to control unmodified ones.[33] Higher expression of integrin molecules in dWJ matrix treated group might be co-related with improved cell migration.[23b] In addition, we speculate that the presence of bioactive growth factors in dWJ matrix, including VEGF, FGF might be responsible for such effects.[23]

Although, the presence of these peptide growth factors in dWJ matrix needs to be investigated to validate the former outcome.

The initial success of cell-free graft relies on faster endothelialization and decorating the graft with NO-producing molecules.[11a,14,34] Rapid cellular migration in the presence of dWJ matrix in vitro is a positive attribute towards graft remodeling, ensuring the functionality of endothelial cells is also a crucial aspect for long-term graft success. In vitro data suggested that dWJ matrix treatment does not significantly alter the proliferation of ECs. However, interestingly, a drastic improvement in ECs′ functionality in terms of NO production and expression of functional markers (CD31, eNOS, and VE-Cadherin) substantiates the usefulness of dWJ matrix. Our observation is in correlation with a prior study reporting the presence of an array of angiogenic factors in WJMSCs secretome (e.g., VEGF, WNT5A, AKT1, CD248, SPON2, etc.), which we assume to be present in the dWJ matrix.[26] Notably, the upregulation of endothelial functional genes, faster cell migration, and increased NO production in the dWJ treatment group validate that our modified decellularization protocol preserves the bioactivity of dWJ matrix. In view of prior reports and our current investigation, it can be established that dWJ matrix is a reservoir of various angiogenic and immunomodulatory factors, which is an encouraging sign towards its application for cell-free vascular grafts.

Another aspect of TEVG remodeling is the degradation rate of implanted material. As of now, there is no general agreement about how fast the material should ideally degrade. Both slow and fast degrading materials have shown the TEVG remodeling and formed mature neo-vessels in animal models.[8a,9] The takeaway point is that the implanted graft should provide enough mechanical stability to allow the formation of neo-vessel without failing. In vitro degradation profile of silk scaffolds in the presence of protease enzyme revealed a faster degradation rate of BAW scaffolds than other controls (Figure 4D). Such behavior could result from the availability of a higher number of enzyme cutting sites in BAW scaffolds due to the intervening dWJ matrix in silk. Notably, none of our implanted silk TEVGs failed due to fast degradation and rupture. Qualitative assessment of the histological cross-sections of explanted TEVGs showed the presence of lesser scaffold struts and dense native tissue comparatively (Figure 7). Therefore, it can be argued that a relatively faster degradation rate of BAW TEVGs concurrently allowed faster neo-tissue formation and remodeling. The former observation is also supported by consistent endothelium and a dense medial layer found in BAW explants. It shows that dWJ functionalized TEVGs could recruit host vascular cells and maintain the vascular tone by providing a functional endothelium layer at the blood-graft interface. In addition, elevated levels of cellular infiltration, be it macrophages or vascular cells, resulted in the production of a higher amount of ECM proteins (collagen and elastin) in dWJ functionalized grafts, which could be correlated with BAW graft mechanical stability in rabbit JV despite a considerably faster degradation rate. Histological images revealed organized collagen deposition on the outside of all silk TEVGs, which might indicate foreign body response leading to fibrous capsule formation.[35] Previous studies suggest that cell infiltration and neo-tissue formation starts in the lumen and ablumen sides of the implanted TEVGs, which traverses through the scaffold walls eventually over time.[36] Dense unorganized collagen deposition observed in the scaffold wall (BAW) suggests the superior chances of these grafts to follow the constructive remodeling pathway, pending future long-term investigation (Figure 7A). On the other hand, the exponential increment of the stress-strain curve of BAW explants is also suggestive of constructive graft remodeling (Figure 9). Comparing biomechanical properties of explanted silk TEVGs with previously reported values for native blood vessels (hSV and pIMA)[30] revealed a comparable strain failure but lower stress failure. In addition, while BM and BA explants showed lower modulus (both toe and linear), the linear modulus of BAW explants was comparable to pIMA (Table 1). The biomechanical properties of TEVG rely on neo-tissue formation.[2] We envisage that a long-term in vivo implantation (≈6 months) of silk TEVGs would facilitate superior mechanical properties.

This study establishes the role of a novel dWJ functionalized silk TEVG towards improved remodeling in a pre-clinical animal model. One of the challenges is to ascertain if the embedded bioactive components of the dWJ matrix vary between donors, which would crucially determine the clinical translation of this technology. Some of the future prospects of the present work might include a detailed proteomic analysis of dWJ matrix to identify the presence of additional cytokines and growth factors participating in the graft remodeling process to understand the underlying mechanism. The rationale behind the adverse effect of higher dWJ concentration (>1mg mL^{-1}) on vascular cells may be investigated. Future studies should explore alternate methods (temperature-induced water vapor annealing,[37] protein self-assembly[38]) of β-sheet transformation in silk scaffolds avoiding the use of organic solvents. Adoption of these all-aqueous approaches is envisaged to preserve the bioactivity of intrinsic dWJ factors with better efficacy. In this study, a small in vivo sample size (n = 3 each group) was investigated for a shorter time (2 months). A long-term in vivo analysis of silk TEVGs with a higher sample size would be required for precluding the possibility of intimal hyperplasia, tracking the graft degradation, and complete neo-vessel formation over time. A few recent studies showed evidence that outcomes of implanted TEVGs differ based on their implantation site,[39] which would be another interesting aspect to investigate.

4. Conclusion

In summary, we developed a novel cell-free TEVG comprised of silk and dWJ matrix. The WJ matrix was decellularized, adopting a modified method to preserve intrinsic bioactive moieties. This is the first report implementing dWJ functionalization of silk vascular grafts. In addition to angiogenic factors, dWJ is also a reservoir of immunomodulatory cytokines (IL-6, IL-8, IL-4, IL-10, and TNF-α). In vitro exposure of dWJ matrix led to the upregulation of endothelial cell functional genes and promoted NO production, which helps in maintaining vascular tone. dWJ treatment also assisted in the faster migration of vascular cells. Downregulation of M1-associated markers and upregulation of M2-associated markers validated the immunomodulatory aspect of dWJ matrix towards the pro-remodeling state, which further assisted in the constructive remodeling of vascular grafts in rabbit JV. The dWJ functionalized TEVGs exhibit 100% patency after two months, shows no sign of calcification, and recruit more host cells (both inflammatory and vascular). BAW grafts also showed consistent

endothelium and a dense medial layer comprising SMCs. Moreover, elevated levels of collagen and elastin indicate constructive graft remodeling. These findings suggest that our composite TEVGs undergo superior remodeling and integrate with the native vessel by modulating the host immune response. We believe that further build-up on our proof of concept study would provide a readily available and clinically viable TEVG.

5. Experimental Section

Preparation and Characterization of Decellularized Wharton's Jelly (dWJ) Matrix: Discarded human umbilical cords (n = 5) were obtained post-delivery from the Guwahati Neurological Research Centre (GNRC) hospital, Guwahati, after due institutional approval (reference no.: Inst/AS/2015/RR-2018/EC-103) and informed patient consent. Cords were transported in sterile ice-cold phosphate-buffered saline (PBS) and processed within 2–3h of procurement. The dWJ matrix was obtained following a previously described protocol with modifications.[23b,24] A schematic representation of the process is shown in Figure 1A. Briefly, the cord tissue was washed thoroughly with sterile Milli-Q water to remove any remaining blood. Post washing, ≈2 cm tissue pieces were treated with red blood cells (RBC) lysis buffer (Sigma Aldrich, USA) for 30 min at room temperature. The amnion membrane was cut open to remove umbilical arteries and a vein from each tissue piece. WJ was scraped and transferred in sterile Milli-Q water (5 tissue pieces in 20 mL water) and kept at 4 °C overnight on a shaker for dissolution. The obtained solution was filtered through a 70-µm strainer to remove any undissolved tissue chunk. The filtrate at this stage contained water solubilized WJ matrix components and MSCs. To obtain the dWJ matrix, cells were removed by centrifugation at 5000 rpm/10 min/4 °C. The supernatant (dWJ matrix) was lyophilized and stored at −20 °C for further use. The DNA content in native and processed tissue was quantified to validate optimal decellularization using Pico green DNA kit (Molecular Probes, USA) following the manufacturer's protocol. Furthermore, the dWJ matrix solution (1 mg mL^{-1}) was prepared in filtered Milli-Q water and subjected for cytokine analysis using a human Bio-Plex Pro Assay kit (Bio-Rad Laboratories, Inc, USA). The kit detects the following human cytokines: GM-CSF, IFN-γ, IL-2, IL-4, IL-6, IL-8, IL-10, and TNF-α. The analysis was performed according to the manufacturer's protocol.

Assessment of Viability and Functionality of dWJ Treated Vascular Cells – Cell Viability: The dWJ matrix was assessed for its compatibility with HUVECs and HDFs at variable concentrations ranging from 0–1mg mL^{-1}. HUVECs (ScienCell Research Laboratories, USA) and HDFs (HiMedia Laboratories, India) were cultured following prescribed protocols and used between P1–P5. dWJ matrix stock solution (5 mg mL^{-1}) was prepared in PBS and sterilized under ultraviolet (UV) light for 20 min. Cell viability analysis in the presence of dWJ matrix was performed using Live-cell staining and measurement of cell metabolic activity (AlamarBlue assay) following established protocols.[40] Briefly, cells were seeded in a 12-well tissue culture plate (10 000 cells/well) for 24 h, followed by dWJ matrix treatment. Live cell imaging was performed using Calcein AM and visualized under a fluorescent microscope (EVOS FL, Life Technologies, USA). In a parallel experiment, the metabolic activity of cells was measured using AlamarBlue assay to quantify the cell viability in the presence of dWJ matrix post 1 and 3 days of treatment. Quantification of cell viability was represented after normalizing with Day 1 value.

Assessment of Viability and Functionality of dWJ Treated Vascular Cells – Expression of Functional Genes (qRT-PCR): Based on the outcome of the biocompatibility assessment of dWJ matrix, 1mg mL^{-1} dWJ was used for all further in vitro 2D experiments. The effect of dWJ matrix treatment on HUVECs was further evaluated by investigating the expression profile of functional genes (CD31, eNOS, vWF, and VE-Cadherin). Cells were cultured in a 6-well plate and treated with dWJ matrix (1mg mL^{-1}) for 24h. Post-treatment, cells were processed for RNA isolation following TRizol based method as described in the previous study.[41] The cDNA was prepared from extracted RNA (200ng μL^{-1} and 260/280 ratio = 1.99–2.01) using a high-efficiency reverse transcription kit (Applied Biosystems, USA) and a thermal cycler. SYBR based standard RT-PCR was performed for target genes using Power SYBR Green PCR master mix (Applied Biosystems, USA) and real-time PCR machine (Applied Biosystems, Quant Studio 5, USA). The primer sequences of the target genes are listed in Table S1, Supporting Information. Relative expression of genes was quantified by $2^{-\Delta Ct}$ method. Human β-actin was used as a housekeeping gene.

Assessment of Viability and Functionality of dWJ Treated Vascular Cells – Cell Migration Assay: The migration of endothelial cells under the influence of dWJ matrix was analyzed by creating a circular wound in the cell monolayer using a polydimethylsiloxane (PDMS) disc (diameter: 2mm, thickness:1mm). A PDMS disc was kept at the center of each well of the 6-well plate, followed by seeding and culture of endothelial cells (10^6 cells/well) in complete growth media until confluence. The PDMS disc was then removed gently without disturbing the cell monolayer, leaving behind a circular blank space (without cells) at the center of the wells. Detached cells were removed by thorough washing with sterile PBS. Culture media (1% v/v fetal bovine serum (FBS)) was replenished in each well, and initial wound images were captured in a phase-contrast microscope. Experimental wells were treated with 1 mg (200 µL aqueous stock) of the sterile dWJ matrix. Images were captured again after 30h culture. Parallelly, HDF migration images were captured following standard scratch assay.[19c] Images were processed using ImageJ to calculate the wound area following the Phase wound plugin (http://dev.mri.cnrs.fr/projects/imagej-macros/wiki/Wound_Healing_Tool). Percent wound closure with time was reported for cell migration analysis.

Assessment of Viability and Functionality of dWJ Treated Vascular Cells – Nitric Oxide (NO) Quantification: Production of NO, a functional molecule responsible for maintaining vascular tone, from HUVEC in response to dWJ treatment was investigated in 2D culture after 6 and 30h following the previous report.[42] A high cell density (3×10^5 cells/well) was cultured in 6 well tissue culture plates, which achieved confluency within a day. After 24h culture, fresh media was added to each well. The Control group was left untreated, while in the experimental group, 200 µL of dWJ stock (1 mg matrix) was added. The culture was incubated for 6 and 30h, and spent media was collected, centrifuged to remove any cell debris, and processed for NO quantification using Griess reagent kit (Thermo Fisher Scientific, USA) following manufacturer's protocol. Fresh cell culture media with and without dWJ matrix was considered as a negative control. The NO concentration was reported after normalization with cell number.

In Vitro Assessment of dWJ Treated Human Monocytes (THP-1) – Cell Viability: THP-1 (human monocyte cell line) was procured from National Centre for Cell Science (NCCS), Pune, India, and maintained in suspension culture in RPMI 1640 media (Sigma Aldrich, USA) following standard culture protocol. THP-1 cells (10 000 cells/well) were cultured in a 96-well tissue culture plate and differentiated to adherent macrophages (M0) by 100 ng mL^{-1} (162 nM) phorbol 12-myristate 13-acetate (PMA) (Sigma Aldrich, USA) treatment for 24h. Cytotoxicity of dWJ matrix at variable concentrations (0–1 mg mL^{-1}) was studied using standard MTT assay following 24h treatment. The viability of THP-1 cells after dWJ treatment (1mg mL^{-1}) was further investigated by fluorescent live-dead imaging by staining cells with Calcein-AM and ethidium homodimer-1 dyes (Invitrogen, USA) following the manufacturer's instructions.

In Vitro Assessment of dWJ Treated Human Monocytes (THP-1) – Immunomodulation Analysis: Considering the presence of immunomodulatory cytokines in dWJ matrix, its ability was looked into to modulate macrophage polarization. THP-1 cells were differentiated into adherent macrophages followed by dWJ treatment (1 mg mL^{-1}) for 24h. Qualitative analysis of immunomodulation was studied by immunofluorescent staining of cells with CD68, CCR7, and CD163 (1:100, Abcam) primary antibodies, and corresponding AlexaFlour 488, FITC tagged secondary antibodies (1:200, Abcam) following standard protocol. Images were captured using a fluorescent microscope. Fluorescence images (n = 6 per group) were further processed to quantify the expression of specific markers using ImageJ software following the previously reported methodology.[21] Expression of phenotype-specific genes (TNFα, CCR7, IL-6, MCP1, and IL-10) was further quantified using qRTPCR following the protocol, as mentioned earlier, to

ascertain the effect of dWJ treatment on human macrophage phenotype modulation. Primer sequences of genes are listed in Table S1, Supporting Information.

Fabrication and Characterization of Silk TEVGs: The aqueous SF protein was obtained from BM cocoons and AA silk glands following established protocols.[40a,43] Tubular bi-layered silk scaffolds were prepared using 3D printed molds following the previously published methodology.[21] Scaffold variants used in this study were composed of different inner porous layers as follows: 1) BM-6% BM, 2) BA: 1:1 ratio of 10% BM and 2% AA, and 3) BAW: BA + 3 mg mL^{-1} dWJ matrix. The choice of using a blend of BM and AA was motivated considering the limitation associated with AA silk, which formed hydrogel at higher concentrations (>3%). To maintain the structural similarity among different experimental groups, the same final concentration (6%, w/v) was used to fabricate the inner porous layer. The inner layer of all three scaffold types (BM, BA, and BAW) were coated with the same outer nanofibrous electrospun layer, following the previous study.[21] The electrospinning solution was consisted of 1:1 (v/v) ratio of 10% (w/v) BM silk and 10% (w/v) PCL (Mn 80 000, Sigma Aldrich, USA) dissolved in 1,1,1,3,3,3- Hexafluoro-2-propanol (HFP, Sigma Aldrich, USA). BAW scaffolds were crosslinked using ethyl(dimethylaminopropyl) carbodiimide/N-hydroxysuccinimide (EDC/NHS) prepared in 80% (v/v) ethanol for 12h.[25c] The crosslinked scaffolds were washed in sterile water on a shaker for 12h and stored at 4 °C until further use. Similarly, stable crosslinking of dWJ matrix component (collagen I) was investigated in scaffold cross-sections by immunofluorescence analysis following standard protocol. Histological sections of bare scaffolds (without cells, after crosslinking step) were treated with anti-human Col-I primary antibody (1:100, Abcam) followed by fluorescent tagging with secondary antibody (Alexa Fluor 488, 1:500, Abcam). Images were captured using a fluorescent microscope.

For morphological analysis, scaffold cross-sections were obtained using a fine blade, preventing any morphological alteration. The surface morphology of silk scaffolds was analyzed under a field emission scanning electron microscope (FESEM, Zeiss, Sigma) after gold sputtering. Captured FESEM images were further processed using ImageJ software to calculate pore size distribution and wall thickness (n = 6 images processed per experimental group). In vitro scaffold degradation in the presence and absence of protease enzyme was quantified following the previously published protocol.[21] Scaffold discs were prepared as described in "In vivo immunomodulation analysis of 3D silk scaffolds" and investigated for swelling and protein release profile following the previous study.[44] Briefly, protein release from silk scaffolds was assessed following the Bradford method. Silk scaffolds of uniform dry weight (approximately 10 mg, n = 6 for each experimental group) were incubated in 1 mL PBS at 37 °C. At predefined time-points, releasates (20µL) were incubated in 200 µL Bradford reagent for 20 min, followed by spectrophotometric analysis at 525 nm. The following standard formula was implemented to calculate the protein release overtime:

$$\text{Protein release } (\%w/w) = (C_2/C_1) * 100 \quad (1)$$

C_1 represents the initial dry weight (mg) of the scaffold and C_2 represents protein content (mg) released over time.

The biocompatibility of 3D silk scaffolds with HUVEC cells was analyzed. Scaffold discs (2 mm thickness, 6 mm diameter) were prepared for all three variants. Sterilized scaffolds were conditioned with the culture media overnight in a 24-well plate and seeded with 10^5 cells (HUVEC) per scaffold. At predefined time points, the cellular metabolic activity was assessed using AlamarBlue assay.[43] The percentage Alamar reduction value was quantified at each time point, and results were reported after normalization with day 1 value. HDF migration was also checked in 3D porous scaffolds. Rectangular scaffold strips (length: 8–10mm, width: 1mm, height: 1mm, n = 3 each) were seeded with ≈10 000 HDF cells at each longitudinal end and cultured for up to 7 days. At predefined time points, scaffolds were treated with MTT [3-(4,5-dimethylthiazol-2-yl)-2,5-diphenyltetrazolium bromide] for 4 h following the previously described protocol.[45] The resulting blue formazan crystals indicated the boundaries of cell growth. The macroscopic images were captured and processed using ImageJ software to calculate the % area coverage over time.

In Vivo Immunomodulation Analysis of 3D Silk Scaffolds: All animal studies were performed post approval from the animal ethical committee (IAEC), West Bengal University of Animal & Fishery Sciences, Kolkata vide permit no. Pharma/IAEC/163. Female adult New Zealand rabbits (1500–2000 g of body weight) were used for subcutaneous implantation of silk scaffolds. 3D silk scaffolds (BM, BA, and BAW, a composition similar to inner layers of silk TEVGs) were prepared by molding the aqueous solution in plastic molds, keeping a 2 mm solution height. Molds were kept at −20 °C overnight and lyophilized for 24h. Circular discs were cut using a biopsy punch (6 mm diameter, 2 mm thickness). Sterilized scaffold discs were soaked in PBS and implanted subcutaneously on the rabbit's dorsal side for five days (n = 3 for each group) and one month (n = 3 for each group). Scaffolds were explanted at predefined time points. Half a portion of each explant was fixed in neutral buffered formalin (NBF, Sigma Aldrich, USA) and incubated with 30% (w/v) sucrose for 2h followed by cryosectioning to obtain 5 µm sections. Histological sections were stained with hematoxylin & eosin (H&E, Merck, USA) following standard protocol. In addition, the immunohistological analysis was performed by staining samples with anti CD68, anti CD163, and anti CCR7 primary antibodies (1:100 dilution, Abcam) followed by treatment with AlexaFlour 488 and DyLight 594 tagged corresponding secondary antibodies (1:200, Abcam). All sections were counterstained with DAPI, mounted, and imaged using a fluorescent microscope. The remaining half of each sample was stored in RNA later (Sigma Aldrich, USA). Tissue samples were homogenized and processed for qRTPCR for the following genes: β-actin, IL-1β, IL-6, IL-10, TNFα, and TGFβ. Primer sequences of genes are listed in Table S1, Supporting Information.

Implantation of Silk Conduits in Rabbit Jugular Vein as Interposition Graft: Female adult New Zealand rabbits (1500–2000 g of body weight) were used for silk scaffold implantation. A total of 9 rabbits were used for this study. Animals were divided into three groups (3 each), and each group received BM, BA, and BAW silk grafts, respectively. Scaffold lumen diameter was selected to match the diameter of the rabbit JV. Anesthesia was induced using xylazine hydrochloride at 5mg kg^{-1} body weight and ketamine hydrochloride at 33 mg kg^{-1} body weight. The Neck portion of the animal was shaved, and an incision was made to expose the internal JV. It was further bisected using micro scissors between microvascular clamps. The silk scaffold was anastomosed with proximal and distal segments of the internal JV in an end-to-end manner as an interposition graft with 10-0 Ethilon following the microvascular anastomosis technique. Once the graft was secured and no blood leakage was observed at anastomotic sites, micro clamps were released. The restoration of blood flow was evaluated and confirmed by the appearance of the venous pulse. The skin and muscle layer were closed using 3-0 polyglactin sutures (McKesson, Richmond, Va). Post-surgery, animals were subcutaneously injected with buprenorphine hydrochloride (0.5 mg kg^{-1}) every 12 h until three days.

Post-operatively, graft patency was monitored by color Doppler imaging after day 12 and day 60 (at the time of graft retrieval). The middle portion of explants was used for histological analysis, whereas ≈1mm tissue section from the proximal, middle, and distal portion from each explant were subjected for ECM proteins (collagen and elastin) quantification. To assess host cell infiltration in silk grafts, 5 µm cryosections were stained for H&E staining. Furthermore, tissue cryosections were also stained with DAPI (Sigma Aldrich, USA) to visualize the cell nucleus. Brightfield images of H&E stained sections and fluorescent images of DAPI stained sections were captured using a fluorescence microscope. Infiltrated cells were quantified by processing the DAPI stained images using ImageJ software following the previously published protocol.[21]

Graft Remodeling and Deposition of ECM Proteins: Histological sections of explanted TEVGs were mounted on coated slides and processed for H&E staining (for cellular distribution), Masson's trichrome staining kit (Sigma Aldrich, USA) (for collagen), and Elastic stain kit (Modified Verhoeff Van Gieson Elastic Stain Kit, Sigma Aldrich, USA) (for elastin) following manufacturer's protocols. Tissue explants were further processed for quantification of ECM proteins: Collagen (Hride Tullberg–Reinert method)[40a] and Elastin (Ninhydrin assay)[21,46] using previously

published protocols. Native rabbit JV was also processed and considered as the positive control. The results of collagen and elastin quantification were presented after normalizing with initial wet tissue weight. Bare silk scaffolds were also processed as the negative control. Infiltration of host vascular cells into graft during remodeling was detected by immunostaining with cell-specific antibodies (calponin and αSMA for SMCs, CD31 for endothelial cells) (1:100, Abcam) using Vectastain Elite ABC Universal kit (Vactor laboratories) following manufacturer's protocol. Stained sections were imaged in the brightfield mode of the microscope (Nikon ECLIPSE Ti2). The presence of resident macrophages was further studied by immunofluorescence staining of explant sections using anti CD68, anti CD163, and anti CCR7 antibodies followed by counterstaining with corresponding secondary antibodies and DAPI. Stained microscopic images were processed per the previous report to quantify the percent area coverage[21] and M2/M1 macrophage phenotype ratio.

Biomechanical Analysis of Silk TEVG Explants: Uniaxial circumferential biomechanical testing of silk TEVG explants was performed in accordance with the previously described methodology.[21] Briefly, 2 mm long circular tissue rings were obtained from the proximal, middle, and distal part of TEVG explant (n = 6), and mounted in two U-shaped stainless steel hooks (rod diameter: 0.5mm) through the lumen connected to pneumatic grips of universal testing machine (UTM, Instron 5944, USA). Samples were pre-conditioned at 5% strain for 10 cycles, followed by recording load-displacement data at 2 mm min^{-1} crosshead speed until failure in hydrated conditions. Stress-strain curves, modulus at low (toe modulus) and high stretch regions (linear modulus), stress, and strain at failure points were further calculated as described previously.[21,47]

Statistical Analysis: Statistical significance of all data was analyzed using Origin 8.0 software following one-way analysis of variance (ANOVA). Analysis of equal variance was performed using the Levene test and mean comparison between groups was performed using post hoc Tukey's test. Two experimental groups were considered significantly different, having *p*-values less than 0.05. All experimental data were acquired for at least n = 3 samples (both biological and technical replicates), unless otherwise noted, and reported as mean ± standard deviation (SD).

Supporting Information

Supporting Information is available from the Wiley Online Library or from the author.

Acknowledgements

P.G. and G.R.C. contributed equally to this work. B.B.M acknowledges funding support from the Department of Biotechnology (DBT), and the Department of Science and Technology (DST) Government of India. P.G. and G.J. acknowledge the Ministry of Education, Government of India for the scholarship. B.B.M., P.G., and G.J. acknowledge Central Instrument Facility (CIF), Indian Institute of Technology Guwahati for providing high-end instruments. D.G. and S.K.N. acknowledges the support of the Honorable Vice-Chancellor of WBUAFS. The authors have filed an Indian patent (patent application number 201931024432, dated June 16, 2020) for this work.

Conflict of Interest

The authors declare no conflict of interest.

Data Availability Statement

Research data are not shared.

Keywords

cell-free vascular grafts, human Wharton's jelly, remodeling, silk, tissue engineering

Received: April 17, 2021
Revised: July 12, 2021
Published online:

[1] P. Gupta, B. B. Mandal, *Adv. Funct. Mater.* **2021**, 2100027.
[2] C. E. Stowell, Y. Wang, *Biomaterials* **2018**, *173*, 71.
[3] a) J. D. Roh, R. Sawh-Martinez, M. P. Brennan, S. M. Jay, L. Devine, D. A. Rao, T. Yi, T. L. Mirensky, A. Nalbandian, B. Udelsman, *Proc. Natl. Acad. Sci. U. S. A.* **2010**, *107*, 4669; b) T. Shin'oka, G. Matsumura, N. Hibino, Y. Naito, M. Watanabe, T. Konuma, T. Sakamoto, M. Nagatsu, H. Kurosawa, *J. Thorac. Cardiovasc. Surg.* **2005**, *129*, 1330; c) N. Hibino, E. McGillicuddy, G. Matsumura, Y. Ichihara, Y. Naito, C. Breuer, T. Shinoka, *J. Thorac. Cardiovasc. Surg.* **2010**, *139*, 431.
[4] J. H. Lawson, M. H. Glickman, M. Ilzecki, T. Jakimowicz, A. Jaroszynski, E. K. Peden, A. J. Pilgrim, H. L. Prichard, M. Guziewicz, S. Przywara, *Lancet* **2016**, *387*, 2026.
[5] A.-M. Kajbafzadeh, R. Khorramirouz, S. M. Kameli, K. Fendereski, S. S. Daryabari, S. M. Tavangar, B. A. Garajegayeh, *J. Thorac. Cardiovasc. Surg.* **2019**, *157*, 1494.
[6] P. Mallis, E. Michalopoulos, A. Dinou, M. S. Vlachou, E. Panagouli, A. Papapanagiotou, E. Kassi, C. S. Giokas, *Hum. Immunol.* **2018**, *79*, 855.
[7] L. Dall'Olmo, I. Zanusso, R. Di Liddo, T. Chioato, T. Bertalot, E. Guidi, M. T. Conconi, *Biomed Res. Int.* **2014**, *2014*, 685426.
[8] a) W. Wu, R. A. Allen, Y. Wang, *Nat. Med.* **2012**, *18*, 1148; b) M. Zhu, Y. Wu, W. Li, X. Dong, H. Chang, K. Wang, P. Wu, J. Zhang, G. Fan, L. Wang, *Biomaterials* **2018**, *183*, 306; c) M. Eilenberg, M. Enayati, D. Ehebruster, C. Grasl, I. Walter, B. Messner, S. Baudis, P. Potzmann, C. Kaun, B. K. Podesser, J. Wojta, H Bergmeister, *Eur. J. Vasc. Endovasc. Surg.* **2019**, *59*, 643; d) R. D. Kirkton, M. Santiago-Maysonet, J. H. Lawson, W. E. Tente, S. L. Dahl, L. E. Niklason, H. L. Prichard, *Sci. Transl. Med.* **2019**, *11*, eaau6934.
[9] J. Fu, X. Ding, C. E. Stowell, Y.-L. Wu, Y. Wang, *Biomaterials* **2020**, *257*, 120251.
[10] M. Rafique, T. Wei, Q. Sun, A. C. Midgley, Z. Huang, T. Wang, M. Shafiq, D. Zhi, J. Si, H. Yan, *Biomaterials* **2021**, *271*, 120746.
[11] a) R. J. Smith, B. Nasiri, J. Kann, D. Yergeau, J. E. Bard, D. D. Swartz, S. T. Andreadis, *Nat. Commun.* **2020**, *11*, 1622; b) B. Nasiri, S. Row, R. J. Smith Jr, D. D. Swartz, S. T. Andreadis, *Adv. Funct. Mater.* **2020**, *30*, 2005769.
[12] D. Hao, Y. Fan, W. Xiao, R. Liu, C. Pivetti, T. Walimbe, F. Guo, X. Zhang, D. L. Farmer, F. Wang, *Acta Biomater.* **2020**, *108*, 178.
[13] M. Wen, D. Zhi, L. Wang, C. Cui, Z. Huang, Y. Zhao, K. Wang, D. Kong, X. Yuan, *ACS Appl. Mater. Interfaces* **2020**, *12*, 6863.
[14] H. Qiu, P. Qi, J. Liu, Y. Yang, X. Tan, Y. Xiao, M. F. Maitz, N. Huang, Z. Yang, *Biomaterials* **2019**, *207*, 10.
[15] R. Daum, D. Visser, C. Wild, L. Kutuzova, M. Schneider, G. Lorenz, M. Weiss, S. Hinderer, U. A. Stock, M. Seifert, *Cells* **2020**, *9*, 778.
[16] Y. Duan, S. Yu, P. Xu, X. Wang, X. Feng, Z. Mao, C. Gao, *Acta Biomater.* **2019**, *96*, 137.
[17] X. Liang, Y. Ding, Y. Zhang, H.-F. Tse, Q. Lian, *Cell Transplant.* **2014**, *23*, 1045.
[18] E. M. Cunnane, J. S. Weinbaum, F. J. O'Brien, D. A. Vorp, *Front. Cardiovasc. Med.* **2018**, *5*, 86.
[19] a) Y. Wei, Y. Wu, R. Zhao, K. Zhang, A. C. Midgley, D. Kong, Z. Li, Q. Zhao, *Biomaterials* **2019**, *204*, 13; b) W. Chen, M. Yang, J. Bai, X. Li, X. Kong, Y. Gao, L. Bi, L. Xiao, B. Shi, *Macromol. Biosci.* **2018**, *18*, 1700242; c) E. M. Cunnane, K. L. Lorentz, A. K. Ramaswamy, P. Gupta, B. B. Mandal, F. J. O'Brien, J. S. Weinbaum, D. A. Vorp, *ACS Appl. Mater. Interfaces* **2020**, *12*, 26955.
[20] J. D. Drews, V. K. Pepper, C. A. Best, J. M. Szafron, J. P. Cheatham, A. R. Yates, K. N. Hor, J. C. Zbinden, Y.-C. Chang, G. J. Mirhaidari, A. B.

Ramachandra, S. Miyamoto, K. M. Blum, E. A. Onwuka, J. Zakko, J. Kelly, S. L. Cheatham, N. King, J. W. Reinhardt, T. Sugiura, H. Miyachi, Y. Matsuzaki, J. Breuer, E. D. Heuer, T. A. West, T. Shoji, D. Berman, B. A. Boe, J. Asnes, M. Galantowicz, G. Matsumura, N. Hibino, A. L. Marsden, J. S. Pober, J. D. Humphrey, T. Shinoka, C. K. Breuer, *Sci. Transl. Med.* **2020**, *12*, eaax6919.

[21] P. Gupta, K. L. Lorentz, D. G. Haskett, E. M. Cunnane, A. K. Ramaswamy, J. S. Weinbaum, D. A. Vorp, B. B. Mandal, *Acta Biomater.* **2020**, *105*, 146.

[22] S. Jadalannagari, G. Converse, C. McFall, E. Buse, M. Filla, M. T. Villar, A. Artigues, A. J. Mellot, J. Wang, M. S. Detamore, *PLoS One* **2017**, *12*, e0172098.

[23] a) K. Sobolewski, A. Małkowski, E. Bańkowski, S. Jaworski, *Placenta* **2005**, *26*, 747; b) P. Dan, É. Velot, G. Francius, P. Menu, V. Decot, *Acta Biomater.* **2017**, *48*, 227.

[24] N. Bakhtyar, M. G. Jeschke, E. Herer, M. Sheikholeslam, S. Amini-Nik, *Stem Cell Res. Ther.* **2018**, *9*, 193.

[25] a) B. Beiki, B. Zeynali, E. Seyedjafari, *Mater. Sci. Eng., C* **2017**, *78*, 627; b) R. W. Chan, M. L. Rodriguez, P. S. McFetridge, *Tissue Eng., Part A* **2009**, *15*, 3537; c) M. Kehtari, B. Beiki, B. Zeynali, F. S. Hosseini, F. Soleimanifar, M. Kaabi, M. Soleimani, S. E. Enderami, M. Kabiri, H. Mahboudi, *J. Cell. Biochem.* **2019**, *120*, 6683; d) D. Li, G. Chiu, B. Lipe, R. A. Hopkins, J. Lillis, J. M. Ashton, S. Paul, O. S. Aljitawi, *Blood Adv.* **2019**, *3*, 1011.

[26] D. Kehl, M. Generali, A. Mallone, M. Heller, A.-C. Uldry, P. Cheng, B. Gantenbein, S. P. Hoerstrup, B. Weber, *npj Regener. Med.* **2019**, *4*, 8.

[27] P. R. Amable, M. V. T. Teixeira, R. B. V. Carias, J. M. Granjeiro, R. Borojevic, *Stem Cell Res. Ther.* **2014**, *5*, 53.

[28] M. M. De Santis, H. N. Alsafadi, S. Tas, D. A. Bölükbas, S. Prithiviraj, I. A. Da Silva, M. Mittendorfer, C. Ota, J. Stegmayr, F. Daoud, *Adv. Mater.* **2021**, *33*, 2005476.

[29] P. M. Crapo, T. W. Gilbert, S. F. Badylak, *Biomaterials* **2011**, *32*, 3233.

[30] L. Soletti, Y. Hong, J. Guan, J. J. Stankus, M. S. El-Kurdi, W. R. Wagner, D. A. Vorp, *Acta Biomater.* **2010**, *6*, 110.

[31] P. Graney, S. Ben-Shaul, S. Landau, A. Bajpai, B. Singh, J. Eager, A. Cohen, S. Levenberg, K. Spiller, *Sci. Adv.* **2020**, *6*, eaay6391.

[32] C. E. Witherel, D. Abebayehu, T. H. Barker, K. L. Spiller, *Adv. Healthcare Mater.* **2019**, *8*, 1801451.

[33] W. Zheng, Z. Wang, L. Song, Q. Zhao, J. Zhang, D. Li, S. Wang, J. Han, X.-L. Zheng, Z. Yang, *Biomaterials* **2012**, *33*, 2880.

[34] S. Dimitrievska, J. Wang, T. Lin, A. Weyers, H. Bai, L. Qin, G. Li, C. Cai, A. Kypson, N. Kristofik, *Adv. Funct. Mater.* **2020**, *30*, 1908963.

[35] A. E. Thurber, F. G. Omenetto, D. L. Kaplan, *Biomaterials* **2015**, *71*, 145.

[36] S. Row, H. Peng, E. M. Schlaich, C. Koenigsknecht, S. T. Andreadis, D. D. Swartz, *Biomaterials* **2015**, *50*, 115.

[37] X. Hu, K. Shmelev, L. Sun, E.-S. Gil, S.-H. Park, P. Cebe, D. L. Kaplan, *Biomacromolecules* **2011**, *12*, 1686.

[38] D. Yao, H. Liu, Y. Fan, *RSC Adv.* **2016**, *6*, 61402.

[39] T. Sologashvili, S. A. Saat, J.-C. Tille, S. De Valence, D. Mugnai, J. P. Giliberto, J. Dillon, A. Yakub, Z. Dimon, R. Gurny, *Eur. J. Pharm. Biopharm.* **2019**, *139*, 272.

[40] a) P. Gupta, M. Kumar, N. Bhardwaj, J. P. Kumar, C. Krishnamurthy, S. K. Nandi, B. B. Mandal, *ACS Appl. Mater. Interfaces* **2016**, *8*, 15874; b) N. Saha, R. Shah, P. Gupta, B. B. Mandal, R. Alexandrova, M. D. Sikiric, P. Sáha, *Mater. Sci. Eng., C* **2019**, *95*, 440.

[41] P. Gupta, J. C. Moses, B. B. Mandal, *ACS Biomater. Sci. Eng.* **2019**, *5*, 933.

[42] Z. Yang, Q. Tu, M. F. Maitz, S. Zhou, J. Wang, N. Huang, *Biomaterials* **2012**, *33*, 7959.

[43] P. Gupta, M. Adhikary, M. Kumar, N. Bhardwaj, B. B. Mandal, *ACS Appl. Mater. Interfaces* **2016**, *8*, 30797.

[44] G. Janani, S. K. Nandi, B. B. Mandal, *Acta Biomater.* **2018**, *67*, 167.

[45] S. Bhowmick, A. Jana, K. Singh, P. Gupta, A. Gangrade, B. B. Mandal, N. Das, *Inorg. Chem.* **2017**, *57*, 3615.

[46] a) E. M. Cunnane, A. K. Ramaswamy, K. L. Lorentz, D. A. Vorp, J. S. Weinbaum, *Bioengineering* **2021**, *8*, 51; b) A. K. Ramaswamy, R. E. Sides, E. M. Cunnane, K. L. Lorentz, L. M. Reines, D. A. Vorp, J. S. Weinbaum, *Matrix Biol. Plus* **2019**, *4*, 100014.

[47] E. M. Cunnane, K. L. Lorentz, L. Soletti, A. K. Ramaswamy, T. K. Chung, D. G. Haskett, S. K. Luketich, E. Tzeng, A. D'Amore, W. R. Wagner, J. S. Weinbaum, D. A. Vorp, *Front. Bioeng. Biotechnol.* **2020**, *8*, 597847.

Biotechnology Advances 34 (2016) 1305–1317

Contents lists available at ScienceDirect

Biotechnology Advances

journal homepage: www.elsevier.com/locate/biotechadv

Research review paper

Understanding osteomyelitis and its treatment through local drug delivery system

Samit Kumar Nandi [a,*], Samiran Bandyopadhyay [b], Piyali Das [a], Indranil Samanta [c], Prasenjit Mukherjee [d], Subhasis Roy [e], Biswanath Kundu [f,*]

[a] Department of Veterinary Surgery and Radiology, West Bengal University of Animal and Fishery Sciences, Kolkata, India
[b] Eastern Regional Station, Indian Veterinary Research Institute, Kolkata, India
[c] Department of Veterinary Microbiology, West Bengal University of Animal and Fishery Sciences, Kolkata, India
[d] Department of Teaching Veterinary Clinical Complex, West Bengal University of Animal and Fishery Sciences, Mohanpur, India
[e] Subject Matter Specialist, Krishi Vigyan Kendra, Nimpith, India
[f] Bioceramics and Coating Division, CSIR-Central Glass and Ceramic Research Institute, Kolkata, India

ARTICLE INFO

Article history:
Received 16 June 2016
Received in revised form 12 September 2016
Accepted 27 September 2016
Available online 28 September 2016

Keywords:
Osteomyelitis
Pathophysiology
Biodegradable carriers
Non-biodegradable carriers
Local antibiotic delivery system
Drug release

ABSTRACT

Chronic osteomyelitis is a major challenge in bone surgery. Conventional use of antibiotics is not an effective way to control the malaise due to so many reasons. Determination of optimal treatment strategy becomes difficult for the orthopaedic surgeons and as a consequence, the patients suffer not only from therapeutic failure but also due to adverse side effects of antibiotics and financial loss due to additional stay at hospitals. A wide application of carrier systems, as a medium for local delivery of antibiotics, is being used experimentally and clinically for the treatment of osteomyelitis. This kind of delivery system provides sustained higher concentration of antibiotics at the infection site with reduced possibility of toxicity. This review highlight etiology and pathophysiology of osteomyelitis, current therapeutic options with their limitations, and potentiality of biomaterial based carrier materials impregnated with antibiotics as local delivery approach.

Contents

1. Introduction

Osteomyelitis is developed by the pyogenic bacteria along with certain strains of mycobacteria and fungi. It involves the inflammation and

* Corresponding authors.
E-mail addresses: samitnandi1967@gmail.com (S.K. Nandi), biswa_kundu@rediffmail.com (B. Kundu).

http://dx.doi.org/10.1016/j.biotechadv.2016.09.005
0734-9750/

subsequent bone loss and spreading of bacterial infection to the soft tissues present alongside (Patzakis and Zalavras, 2005).

It has three sub divisions *viz.*, acute (develops within 10 days), sub-acute (develops within two weeks to month) and chronic forms (after several months) of the disease. Acute osteomyelitis may develop as a result of bacterial presence in blood, particularly in elderly patients and prepubertal children (Lew and Waldvogel, 2004) with edema, local anoxia and pus formation. Hematogenous osteomyelitis may ensue before the occurrence of osteonecrosis (Lew and Waldvogel, 2004). It has been reported that occurrence of hematogenous or acute osteomyelitis is more (>85% of cases) in the children below the age group of 17 (Mader et al., 1999a). Chronic osteomyelitis is evident with osteonecrosis, formation of a large area of devascularized sequestrum and generally develops from untreated or improperly treated acute phase (Lindfors et al., 2010).

Antibiotic therapy is the traditional choice for treatment of osteomyelitis. Number of antibiotics presently exists to treat this condition. Nevertheless, as per the doctors, no fruitful solution of this situation found due to ever-rising bacterial resistance after antibiotic use in bed side (Philippe Bidault et al., 2007). Besides, the local ischemic condition and presence of "blood–bone" barrier lead to poor penetration of antibiotic in the site of interest.

Local delivery of antibiotics have emerged as newer therapeutic modalities to overcome the limitations as well as effective management of osteomyelitis cases. Availability of high concentration of antibiotics in an avascular zone justifies its local site use. Besides, high concentrations are also of paramount necessity to destroy the remaining organisms in biofilms. Regardless of the acceptance of these therapeutic modalities, solving their use in a biofilm environment is sought for. Scientific approaches are underway for overcoming such frustrating maladies. Therefore, attention of this review is based on its classification, pathophysiology, conventional management approaches and their limitations and recent paradigm shift. We describe antimicrobial agents for osteomyelitis therapy with special reference to release kinetics, biodistribution, drug metabolism, and presently investigated delivery vehicles.

2. Risk factors and incidence of osteomyelitis

The etiological bacterial profile differs with the susceptible age groups. The susceptible age groups include infants, children, and adults. More frequently, children are victim with the development of pain and tenderness over affected bone along with other systemic problems like fever, inability or difficulty in using concerned limb especially during walking or bearing weight (Hartwig, 2006). On the contrary, in adults symptoms develop slowly that include fever, nausea and reddening of the concerned bone.

Mostly, adults over the age of 50 years (except intravenous drug users) are the victim by this disease (Chandrasekar and Narula, 1986) and it accounts nearly 15% (Waldvogel et al., 1970). However, people suffering from diabetes, peripheral neuropathy or vascular disease do not show any symptoms (no pain or fever) other than an unhealed skin wound which is worsening gradually (King, 2015). Application of foreign materials and bone damage due to trauma or/and exposure to a large bacterial inoculation can lead to osteomyelitis prevalently; although, infection of bone is found to be very rare (Eid and Berbari, 2011). The higher possibilities of osteomyelitis include patients suffering from diabetes, aging, hepato-renal failure, immune-suppression *etc.* (Eid and Berbari, 2011). It has been reported that the infection rate is lowest after primary joint replacement (1%) (Phillips et al., 2006) to open fractures (23%) (Patzakis and Wilkins, 1989).

3. Pathophysiology

In the pre-antibiotic era, acute osteomyelitis carried 50% mortality due to devastating sepsis and metastatic abscess (Joyner and Smith, 1936). The pathophysiology of osteomyelitis showed that the occurrence of this disease has multiple routes. It can be spreaded by direct bacterial inoculation or air borne contamination as well as hematogenous seeding of bacteria to reach the bone (Gogia et al., 2009). Apart from bacterial infection, fungi also lead to osteomyelitis (Eid and Berbari, 2011). On the basis of the pathogenic mechanisms and the source of infections, osteomyelitis can be divided (Lew and Waldvogel, 2004) into three categories viz. a) that associated with microbial infection due to trauma, surgical operation or incorporation of a prosthetic joint b) that further complicated by vascular insufficiency as may happen in diabetes mellitus and/or peripheral vascular disease patients (Calderini et al., 2014) and c) following hematogenous spread of infection, majority in vertebral osteomyelitis and in children (Carmody et al., 2014).

However, bacteria have different mechanisms to cause infection in the bone once it has entered into the body. It can facilitate infection by cell-cell, cell-implant adhesion causing acute inflammation (Gogia et al., 2009) (Figs. 1–2). In acute infection, microorganisms after entry and being phagocytosed, release toxic oxygen radicals and proteolytic enzymes which cause surrounding tissue lysis (Lew and Waldvogel, 2004). Further, inflammation of surrounding blood vessels leads to increase intraosseous pressure and thereby impairs blood flow to the area. Poor vascular perfusion hindered the penetration of antibiotics vis-a-vis lowers the antibacterial action even under normal dose level.

Ultimately devascularized sequestrum is generated due to the necrosis of bone (Lew and Waldvogel, 2004). As a therapeutic option, intensive debridement of these bone fragments and sequestrum also carried out which leaves a huge cavity in the local site (Xing et al., 2012). *Staphylococcus aureus,* one of the major causative agents of this disease, gets attached to the bone with the help of the expressed receptors (adhesions) for bone matrix components like fibronectin (Maxe et al., 1986), laminin (Herrmann et al., 1988), collagen (Patti et al., 1993), and bone sialoglycoprotein. It has also been reported that the same glycoprotein plays a crucial role to arbitrate bacterial bonding with metal plates and screws (Patti et al., 1993). Therefore, the pathogen gets entry to the cartilage once it is expressed as collagen-binding adhesion (Lew and Waldvogel, 2004; Wright and Nair, 2010). It has been also reviewed that host defense mechanisms and antibiotic therapies are sometimes unable to control the infection due to its diverse mechanisms like maintaining a very slow metabolic rate, living in dormant state inside osteoblast and/or developing a biofilm (Eid and Berbari, 2011; Gould et al., 2012). The microbes pass from a planktonic

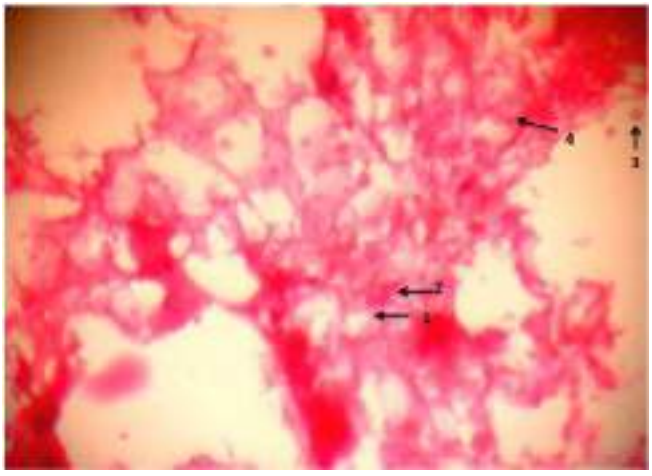

Fig. 1. Histological section of osteomyelitis; 1. bony matrix 2. osteocyte 3. osteoclast 4. immature bony osteoid (with permissions from Springer).

Fig. 2. Radiograph of osteomyelitis of tibia; arrow indicates osteophytic and lytic changes (with permissions from Springer).

phase into a sessile form with a high metabolic rate and rapid multiplication to greatly reduced metabolism and slowed biological reactions. This ultimately reduces their sensitivity to antibiotics by a factor of 10^3. Thus, osteomyelitis poses a constant challenge not only for increase in the number of patients being hospitalized per year but also due to its expenses (Frank et al., 2011).

4. Microorganisms causing osteomyelitis

Typical micro-organisms which usually causes osteomyelitis, is given in Table 1, while pathogenesis of osteomyelitis is schematically represented in (Fig. 3).

(Baker et al., 1987; Calderini et al., 2014; Cooney and Cooney, 2011; Haas and McAndrew, 1996; Marchocki et al., 2013).

Table 1
Microorganisms causing osteomyelitis.

Condition	Causative organism
Chronic osteomyelitis	*S. aureus* is the major followed by pseudomonas and enterobacteriaceae (Haas and McAndrew, 1996). Less frequent micro-organisms are *Salmonella*, *Clostridium* and *Pasteurella multocida* (Baker et al., 1987).
Osteomyelitis involving diabetic foot	Polymicrobial infection (Calderini et al., 2014; Cooney and Cooney, 2011)
Chronic osteomyelitis involving mplants as well as in 90% of pin tract infections	*Staphylococcus epidermidis* (Marchocki et al., 2013)

5. Conventional therapeutic strategies

5.1. Systemic antibiotic therapy in osteomyelitis

Effective antimicrobial therapy constitutes the mainstay for successful treatment of osteomyelitis. However, clinical response to antimicrobials always remains elusive due to numerous factors like poor penetrability of the drugs preventing the drug to attain required minimum inhibitory concentration (MIC) level in bone tissue and prolonged course of therapy. Successful clinical recovery also requires repeated surgical drainage and debridement, thereby making the medical intervention more complicated and infection prone. β-lactam drugs like penicillin, cephalosporins and carbapenems which constitute the mainstay of therapeutic in treating the osteomyelitis, poorly penetrate the bone tissue and bone level of drugs merely achieve 5–20% of the serum level. Following parenteral administration of the some of the β-lactam drugs, bone concentrations remain fairly high exceeding the minimum inhibitory concentration (MIC) against infective micro-organisms in the bone. But that is not what happens when the drugs are prescribed orally as serum level (<10% of the parenteral route) of the drugs rarely achieve the substantial concentration due to poor absorption through gut. In contrast, some of the antibiotics reach appreciable bone concentration following oral administration like clindamycin (used for MRSA infection), fluoroquinones, fosfomycin (used to treat MDR enterobacteriaceae) and metronidazole (for anaerobic infection). The details of the bone concentration of all these drugs are given in Table 2.

Most of the oral therapy of osteomyelitis was done for the fluoroquinone drugs. Among fluroquinones, ciprofloxacin, moxifloxacin and levofloxacin are most commonly used for this purpose and were extensively studied as par as their kinetics and distribution in osseous tissue is concerned. Studies indicated that overall cure rate may reach up to 60–80% with the use of these drugs. Nevertheless, oral therapy for management of osteomyelitis may have to be continued for 12–16 weeks at very high dose. Levofloxacin concentration was determined in different patients undergoing surgery following a single intravenous injection of 500 mg where average concentration of cancellous and cortical bone were 6.6 ± 3.6 mg/g and 2.8 ± 1.1 mg/g, respectively (Baum et al., 2001). In elective total hip replacement, a bolus parenteral injection of levofloxacin (500 mg) was found sufficient to achieve a concentration of the drug in synovial fluid (8.9 ± 2.1 mg/kg), cortical (3.9 ± 1.2 mg/kg) and cancellous (7.4 ± 2.2 mg/kg) bone tissue to cross the breakpoints of susceptible organisms (Rimmele et al., 2004). Levofloxacin and moxifloxacin dispersion into cancellous and cortical bone was studied in total hip arthoplasty patients (Metallidis et al., 2007). It is also observed that moxifloxacin is having mean cancellous penetration of 53.86%, cortical part 41.59% and levofloxacin of 54.13% andin 34.26% respectively (Metallidis et al., 2007). Considerable penetration of moxifloxacin in sternal bone of the patient was 1.45 μg/g at 5 h in the body (Metallidis et al., 2006). Recent study showed around 80% bioavailability of moxiflaoxacin in bone of total hip replacement patients (Landersdorfer et al., 2009). Taken together, fluoroquinone seem to have an appreciable bone penetration to reach a concentration above the MIC of common infectious pathogens and same can be used for treatment of chronic osteomyelitis.

Even though, newer generation cephalosporins have excellent spectrum of antibacterial activity against most of the infective pathogens, they have limited scope in systemic antibacterial therapy in osteomyelitis. A recent study conducted in septic disjoined tibial patients, ceftriaxone penetration (<15%) and concentration in bone were found suboptimal particularly in cortical component (9.6 ± 3.4 mg/L *i.e.*, 7.8%) (Garazzino et al., 2011). Cefuroxime was previously considered as a systemic therapy for osteomyelitis. However, recent studies have confirmed that cefuroxime can hardly achieve sufficient concentrations in cancellous and cortical bone to exert bactericidal properties (Tottrup et al., 2014). In contrast, amoxicillin clavulinic acid combination offered appreciable prophylaxis against post-operative wound infection in hip

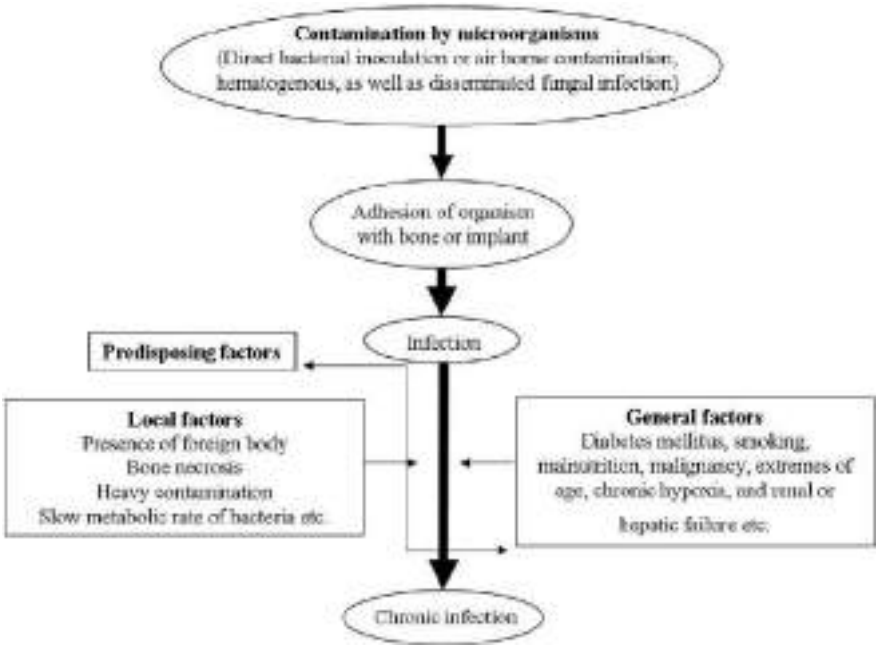

Fig. 3. Schematic representation of pathogenesis of osteomyelitis.

replacement cases. In hip replacement complications patients, it has been observed that if 2.2 g Augmentin was given before surgery, a concentration of 9.2 and 5.9 mg/kg could be achieved in the cortex and spongy layer between 2 and 5 h (Weismeier et al., 1989). Despite the wide scale surfacing of beta lactamase producing enterobacteriaceae, very limited studies were conducted on bone penetration of betalactamse inhibitor potentiated drugs. However, studies have confirmed that piperacillin and tazobactum may be a good alternative in soft tissue and bone infection (Al-Nawas et al., 2008).

Trimethoprim-sulphamethoxazole (TMP-SMX) combination therapy is second only to ciprofloxacin which is also frequently tried for treatment of osteomyelitis or with variable success. It has been reported a cure rate of almost 98% in chronic osteomyelitis using TMP-SMX oral therapy for over 6 months alone with proper surgical debridement (Mader et al., 1999b). Similarly, the use of TMP-SMX alone or combined with linezolid could cure almost >80% of the patients with chronic osteomyelitis (Nguyen et al., 2009). Successful treatment of chronic osteomyelitis was reported with or without orthopaedic implant using oral therapy of TMP-SMX alone or within rifampin and rifampin plus ciprofloxacin for over a period of 10 weeks (Javaloyas and Monreal, 1999). The study pointed out the usefulness of TMP-SMX therapy. It has also been reported a success rate of 60–80% to treat the patients with MRSA infected orthopaedic implants (Stein et al., 1988). The studies thus indicated usefulness of TMP-SMX either alone or in combination for treatment of osteomyelitis.

Glycopeptides like vancomycin and drugs like daptinomycin and teicoplanin which form the inevitable part for treating MRSA or other anaerobic infection in the bone have poor bone penetrability. Previous studies indicated that vancomycin hardly reached to a concentration of 2.3 μg/g of bone following intravenous application of vancomycin @ 15 mg/kg in patients with total hip arthroplasty (Graziani et al., 1988). In another study, penetration of vancomycin and teicoplanin was detected in infected tibial pseudoarthrosis cases (Garazzino et al., 2008). The concentration of vancomycin in cortical and cancellous bone was 2.66 ± 1.2 and 11.53 ± 7.8 mg/L respectively (Garazzino et al., 2008) whereas teicoplanin was much less – 2.01 ± 1.2 and 7.51 ± 7.8 mg/L, respectively. There is paucity of literature on bone penetration of vancomycin in human patients with osteomyelitis with systemic drug therapy in recent years. However, an experimental trial in rabbit with prosthetic device infection revealed that vancomycin penetration may reach up to 53% and 28% of plasma concentration, into the infected bone (femur) and uninfected bone respectively (Swoboda et al., 2009). In general, teicoplanin showed poor bone penetration. To achieve adequate bone concentrations, at least 10 mg/kg dose was necessary (Wilson, 2000).

Daptomycin is an antibiotic of lipopeptide nature and it is used against gram-positive organisms causing systemic and life-threatening infections. Daptomycin showed poor bone penetrability but the bone concentration was found to be sufficiently higher to achieve the bactericidal concentration. Recently a study conducted by Montange et al. in clinical cases of joint replacement revealed that following an intravenous administration of daptomycin @ 8 mg/kg body weight, median percentage penetration in synovial fluid and cancellous bone were 54% and 9% respectively around 8 h (Montange et al., 2014). Daptomycin concentration in hip and shin bone was 3.3 to 3.4 μg/g which was above the MIC break point of clinical *S. aureus* isolate. Thus daptomycin therapy registered a cure rate of 65 to 89% in various cases of osteomyelitis. >75% success rate was recorded in osteomyelitis predominantly in elderly patients following daptomycin therapy. Linezolid is another important bacteriostatic antibiotic with excellent bioavailability (near about 100%). Therefore, linezolid is often used to treat the gram positive infection in osteomyelitis even though bactericidal drugs are often preferred for management of chronic osteomyelitis (Falagas et al., 2007). Recent studies indicated that >80% patients with chronic osteomyelitis may be successfully treated with systemic linezolid therapy (Lu et al., 2010). The presence of linezolid into bone and soft tissue has been determined in methicillin-resistant *Staphylococcus* (MRS) infected patients with intravenous injection of 600 mg (Kutscha-Lissberg et al., 2003). In infected knee or hip joint tissue, bone sample and non-infected bone sample, mean concentration of linezolid were >10 mg/L, 3.9 ± 2 mg/L and 6.3–8.5 mg/L, respectively (Kutscha-Lissberg et al., 2003). A case of total knee replacement revealed average concentration of linezolid 91.9%, 82.2%, 83.5% and 40.1% in synovial fluid, synovium, muscle and bone, respectively (Rana et al., 2002). Mean concentrations of linezolid at 90 min after the final dose (600 mg), in serum, synovial fluid, synovium, muscle and cancellous bone were at least twice the MIC90 for Staphylococci and Streptococci (Rana et al., 2002). Keeping in mind the poor penetrability of glycopeptides and third or fourth generation cephalosporin in the bone, there is an urgent requirement of alternative drugs to tackle the infection caused by MRSA or ESBL producing

Table 2
Common antibiotic used for systemic therapy of osteomyelitis and their kinetics profile (C_{max} denotes time at maximum serum concentration; $t_{1/2}$ represents half-life and V_d denotes volume of distribution).

Drugs	Dose	C_{max} (h)	$t_{1/2}$	Protein binding	V_d	Clearance and metabolism	Serum concentration	Bone concentration	References
Ciprofloxacin	200 mg IV		4–6 h	20–40%	78.41 ± 13.17 L in elderly patients	50–70% through urine as un-metabolized drug and 10% as metabolite; 18.39 ± 4.15 L/h Clearance in aged people	1 < to about 4 mg/kg	1–3 mg/kg (skull bone); 2 mg μg/g (medullary); 1.4 mg μg/g (cortical)	(Cios et al., 2014; Rick et al., 1996)
Levofloxacin	500 mg	2.8 and 5.2 μg/mL within 1–2 h	6–8 h	24 to 38%	1.1 L/kg	87% through urine unmetabolized; <5% in urine as desmethyl and *N*-oxide metabolites	7.5 μg/mL	7.4 (medullary) 3.9 (cortical) (μg/g)	(Fish and Chow, 1997; Rimmele et al., 2004)
Moxifloxacin	400 mg IV	3.4–4.5 within 1–1.5 h	11.5–15.6 h	32% (*in vitro*) 48% otherwise		20% through urine and 25% via faeces and 52% as via glucuronide and sulfate conjugation	4.9	1.9 (medullary) 1.3 (cortical) (μg/g)	(Goudah and Hasabelnaby, 2010; Malincarne et al., 2006; Stass et al., 1998)
Linezolid	600 mg oral	11.99 ± 3.67 μg/mL	Variable 4.71 ± 1.23 h	31% 14.78% (range, 3.85 to 32.03%)	0.71 ± 0.25 L/kg of body weight	Liver by oxidation of morpholine ring Clearance is variable	23	8.5 (μg/g)	(Rana et al., 2002; Wiskirchen et al., 2011)
Daptomycin	4–6 mg/kg	57.8 (3.0) μg/mL 93.9 (6.0) μg/mL	8 h	90–93%	0.096 (0.009) L/kg at steady state	8.3 (1.3) mL/h/kg Mostly by kidney		3.3–3.4 μg/g at hip bone	(Bradley et al., 2014; Montange et al., 2014)
Ceftriaxone	50 mg/kg IV	216 μg/mL within 0.5–1 h	7–8 h	95%	338 mL/kg	0.58–1.45 L/h biliary and renal excretion	104 (1 g IV)	20 (μg/g)	(Lovering et al., 2001)
Ceftizidime		45 and 90 within 20–30 min	1.9 h with IV	<10%		Renal (80–90% unchanged)	150	5 (μg/g)	(Raymakers et al., 1998)
Cefepime			2 h	20%	120 (±8) mL/min		73 ± 24	74 ± 12 (cancellous) 68 ± 16 (cortical) (μg/g)	(Breilh et al., 2003)
Clindamycin	150 mg oral	2.5 μg/mL within 45 min	2.4 h	>90%		Renal and fecal excretion	8.5 (with 600 mg dose)	3.5 (μg/g)	(Schurman et al., 1975)
Metronidazole			8 h	<20%		Renal clearance	34	27 (μg/g)	(Bergan et al., 1985)
Doxycycline			12–24 h	80–90%		Bile and urine	6 (200 mg IV)	0.13 (μg/g)	(Gnarpe et al., 1976)

enterobacteriaceae harboring multiple resistance gene. Fosomycin was proved to exert appreciable antibacterial action against such pathogen especially biofilm producing *Staphylococci*, one of the main offender in osteomyelitis (Shi et al., 2014). This peptide antibiotic due to low plasma protein binding property and low molecular weight may diffuse through tissues and reach the bone at high concentration. A study in diabetic patients with foot infection associated with bacteria, it was revealed that the metatarsal bone concentration may reach up to 100 mg/mL at 3 h with a dose of fosfomycin @ 100 mg/kg body weight (Schintler et al., 2009) (*cf.* Table 2).

(Bergan et al., 1985; Bradley et al., 2014; Breilh et al., 2003; Cios et al., 2014; Fish and Chow, 1997; Gnarpe et al., 1976; Goudah and Hasabelnaby, 2010; Lovering et al., 2001; Malincarne et al., 2006; Montange et al., 2014; Rana et al., 2002; Raymakers et al., 1998; Rick et al., 1996; Rimmele et al., 2004; Schurman et al., 1975; Stass et al., 1998; Wiskirchen et al., 2011).

Nevertheless, except few drugs like fluoroquinones and fosfomycin, the efficacy of systemic antibiotic therapy is not very promising in treating complicated cases of osteomyelitis and prosthetic surgery because of poor penetrability of these drugs during ischemic and necrotic injuries for poor vascularization. Thus treatment may require repeated parenteral administration to maintain adequate concentration of the drugs in the bone and it may require repeated hospital administration and may affect the health of the patient in long run. Thus the main focus of antibiotic therapy relied on using local delivery system.

Keeping this in background antibiotic impregnated bone cement was introduced in orthopaedic surgical management and for treating the cases of osteomyelitis way back in 1970 in Europe. Use of antibiotic impregnated bone cements has many advantages over parenteral or oral application of the drugs. The antibiotic concentration is much higher using the drugs coated beads and the same is maintained for a long duration thus it can favor the healing process in more convenient manner. On the other hand, chance of systemic toxicity which is usual following parenteral administration of the drugs, is reduced using drugs coated beads. Studies have indicated that the occurrence of ototoxicity, nephrotoxicity, and other untoward or adverse hypersensitivity reactions are much diminished in antibiotic coated cement beads. These beads help in increasing the local concentration of the provided drug keeping its systemic or local concentration at minimum level. Moreover, they can fill the dead spaces leftover following surgical debridement.

5.2. Procedures related to surgery

Conventional therapy of osteomyelitis includes surgical debridement, exclusion of implants, necrotic tissues, restitution of blood supply, soft tissue and systemic administration of antibiotics, which becomes successful in up to 90% of cases (Hanssen and Spangehl, 2004; Insall et al., 2002). A long-term systemic antibiotic therapy is the alternate option to overcome such situation but with additional risk of toxicity. Common strategies and their advantages and disadvantages are shown in Table 3.

5.3. Non-biodegradable vs. biodegradable carriers

High systemic doses of antibiotic are of paramount necessity in the affected body part, but, it leads to systemic toxicity. The antibiotics may not produce complete spectrum of activity in sparsely vascularized tissues and osteonecrosis which is often associated with osteomyelitis. Further, normal dose of antibiotics are incapable to penetrate the capsule of the etiological micro-organisms. In spite of all the developments in surgical techniques and new antibiotics with increased spectrum, the management of bone and allied tissue infection is still a difficult task.

A wide application of carrier systems, as a medium for local delivery of antibiotics, is being used experimentally and clinically for osteomyelitis therapy. The modality of treatment has progressed to success due to

Table 3
Common strategies with their respective advantages and disadvantages for long-term systemic antibiotic therapy.

Strategy	Advantages	Disadvantages
Systemic antibiotics therapy	Eradication of bacteria	More side effects, expensive hospital stay and low antibiotic concentration at the interest site leads to resistances.
Surgical removal of sequestra and infected tissue	Successful approach and no untoward toxic side effects	Added surgery needed which may lead to more chance of infection and involvement of costs, radical debridement leads to bone loss and subsequent difficulty in healing.
Local antibiotic delivery	• Minimum or no systemic side effects • Single surgery is sufficient. • Shorter hospital stay and low costs	Resistances due to low antibiotic concentration

its ability to provide sustained higher concentration of drugs at the infection site (Zhang et al., 2010) and in addition to avoiding potential toxicity due to systemic administration of antibiotic. Further, antibiotic concentration can be increased locally more than ten times in comparison to intravenously applied antibiotics (Kanellakopoulou et al., 2009).

Non-biodegradable carriers have been used for delivery of antibiotics in osteomyelitis site since past but have been gradually withdrawn due to some serious adverse effects. The biofilm helps in bacterial immigration and ultimately secondary infection develops. Moreover, due to difficulty of encapsulation of limited variety of antibiotics, the implant has to be removed in a further procedure (Rushton, 1996). On the contrary, the biodegradable carriers are becoming a research focus nowadays due its superior biocompatibility and greater bone restoration properties (Anal and Stevens, 2005). The biodegradable implant is not required to be removed and as a consequence it reduces the possibility of secondary infection. Moreover, biodegradable carriers are having osteogenic potential and flexibility (Catelas et al., 2006) which helps in osteogenesis (Anal and Stevens, 2005).

5.4. Non-biodegradable systems

The cement beads impregnated with antibiotics are used in management of soft tissue and bone infections for last few decades. In 1984, this was first used prophylactically for deep seated bone infection in orthopaedic endoprosthetic surgery in human. Thereafter, it is being used as an effective alternative for sustained and high level antibiotic release at local site for treatment of infection associated with bone and soft tissues. Polymethylmethacrylate (PMMA) is the most frequently used antibiotic coated cement beads for this purpose (Magnan et al., 2013). PMMA is available in two forms – bead cements and bead chains impregnated with antibiotic which are used for management of arthoplasties and musculoskeletal infections, respectively. PMMA is advantageous due to two reasons – PMMA do not trigger any immune response and thus there is no chance of hypersensitive reaction in the host. PMMA in beads provides a wide surface area for release of antibiotics so as to maintain high concentration of the drug *in situ* (Lalidou et al., 2014). Barring this, there are other factors which influence the success of antibiotic coated PMMA.

The elution of antibiotic from PMMA is the most important factor to influence the success of therapeutic intervention by this method. It depends on the type of the cement used for this purpose. Not only that, increased porosity of the beads is also helpful for elution of the drugs. For higher elution of drugs, most useful method is to apply dextran or polyethylene glycol to increase porosity of the beads, thereby increasing the concentration of antibiotics as coating. Again the size of the beads is also important determining factor for elution of drugs. Smaller the size of the beads better will be the elution probably because of more surfaces to volume ratio. Again the surrounding tissue environment and fluid also influences the drug release and elution. The better release of some drugs like vancomycin was observed in high-speed hand mixing bone cement (Pithankuakul et al., 2015).

Two types of PMMA beads are available in the market. In general, commercial beads are uniform and about 7 mm diameter. Non-commercial beads are prepared by the surgeon himself by mixing the antibiotics with the beads. However, lack of uniform size and shape of the beads and improper mixing of the antibiotics are the major drawback of the non-commercial preparation. This often leads to less bioavailability of the antibiotics. However, storage time and temperature of the antibiotic loaded bone cement have role on the drug release as revealed in a recent study using vancomycin loaded PMMA (Chen et al., 2013).

Elution of antibiotic and their bioavailability depend upon selection of suitable antibiotic-type, *e.g.*, stability of drugs at very high temperature, when polymerization of PMMA beads occur alongwith drug. Because of their stability at very high temperature, aminoglycosides including streptomycin, gentamicin, amikacin and tobramycin are the most preferred antibiotics for this purpose and frequently used for impregnation on the bone cement. Other groups of antibiotics like β-lactam drugs of cephalosporin groups, ciprofloxacin and glycopeptide (vancomycin) are also used for this. Moreover, recent reports show effective outcome in combining approach of gentamicin and vancomycin loading in the bone cement (Regis et al., 2013). Surgical drainage fluid and serum concentration of both the drugs maintain sufficient concentration of the drugs to exert inhibitory effect against MRSA and CoNS infection in the bone. Recently, a number of antibiotics like vancomycin, teicoplanin, ceftazidime, imipenem, piperacillin, gentamicin, and tobramycin have been have been loaded with polymethylmethacrylate to assess antibacterial efficacy against multiple pathogens (Chang et al., 2013). Although, antimicrobial action was noticed, longer period of release and a broader antibacterial spectrum was produced by gentamicin than other antibiotics. Thus gentamicin is regarded as one of the potential antibiotic for inclusion in PMMA based bone cements due to its broad spectrum bactericidal activity, water solubility, heat resistance, chemical stability, little sensitization potential and protein binding activity and finally because of minimal chance of resistance development (Webb et al., 2013).

Irrespective of the type of antibiotics, their elution is mostly bimodal. About 5% of loaded drugs release from beads in first 24 h and balance quantity releases over next few weeks or months. Thus the antibiotic concentration in the surrounding medium is very high initially followed by sustained release during the passage of time. Other than the type and concentration of antibiotics, elution of the drugs is also dependent upon the structural characteristics of the bone cement. Despite, the variation among different group of antibiotics, all the drugs displayed adequate elution but maintenance of their sufficient concentration over the subsequent period of time well above to exert bactericidal properties may vary depending upon the type of drugs used as revealed in several experiments. Various experiments showed that for the drugs like quinolones, tobramycin, gentamicin, vancomycin peak concentration is achieved at very first day of application of the bone cements (Galvez-Lopez et al., 2014).

The management of gram-positive infection in osteomyelitis is a crucial concern with recent emergence of methicillin or vancomycin resistant *Staphylococcus aureus*, which left the clinicians with limited therapeutic options. Daptomycin combination with acrylic bone cement was studied in joint arthoplasty surgery (Bradley et al., 2014). Appreciable elution was noted in first day for all the three concentrations *i.e.*, 9.59 ± 0.85%, 15.25 ± 0.69%, and 20.64 ± 20.33% respectively. All the

Fig. 4. Post-operative radiographs and histology of human patients. X-ray radiographs taken post-operatively after 2 months (a), 4 months (b), 6 months (c) and 8 months (d); histology of the antibiotic CFS impregnated HAp (HE × 20) (e) [in Fig. 3e: (1) Haversian canal, (2) neo-vascularization and (3) fibro-vascular structure]; patient standing on his feet unaided after 8 months (f) (with permissions from Elsevier).

formulation also displayed bactericidal property; however, the high concentration encapsulation was more effective (Hsu et al., 2014). In another set of experiment, elution kinetics and antibacterial efficacy of PMMA bone cements with different concentration of daptomycin, vancomycin, and teicoplanin were evaluated against the susceptible and resistant strains of *Staphylococcus aureus* (MSSA) (Lewis, 2009). Amid the studied antibiotics, teicoplanin showed better results against the tested pathogens. Other than MRSA coagulase negative *Staphylococcus* associated biofilms are also associated with chronic osteomyelitis. Recently a study has been conducted using daptomycin/and with gentamicin impregnated PMMA to assess their efficacy against *S. epidermidis* associated biofilms. In the said study, vancomycin proved more efficacies *in vitro* against *staphylococcus*. On the other hand, PMMA in combination with daptomycin and gentamicin completely subdued *S. epidermidis* biofilm creation (Arias et al., 2015). Of late, elution kinetics, mechanical properties and antimicrobial efficacy of diverse antibiotics (impregnated acrylic bone cements) was studied. The antibiotics like vancomycin, gentamicin, daptomycin, moxifloxacin, rifampicin, cefotaxime, cefepime *etc.* were loaded with bone cement (10 or 20% w/w) (Galvez-Lopez et al., 2014). Among these drugs vancomycin, gentamicin, rifampicin and moxifloxacin showed excellent results with sustained and high elution rates for the entire experimental period and maintain the *in situ* antimicrobial efficacy. On the other hand, elution rate of etrapenem, meropenem, daptinomycin and cefotaxime decreased from 4th day onwards. However, the concentration of ampicillin, amoxicillin clavulanate and cefotaxime decreased rapidly and was barely detectable (Galvez-Lopez et al., 2014). Very few studies have been done on elution kinetics of antifungal and their bio-active properties following their delivery through antimicrobial loaded bone cement. However, it is important to know about local delivery and sustenance of antifungal to control the joint infection. Previous studies on elution kinetic of amphotericin B showed that the drug could be barely detected beyond one week in the local site (Goss et al., 2007). In contrast, ALBC loaded with voriconazole seems to offer appreciable bioavailability at the local site. Almost 60–75% of the drug is being released using 300–600 mg formulation of voriconazole by 30th day of drug implantation. The experiment highlighted that 300 mg of voriconazole in ALBC could deliver meaningful amounts of active drug *in vivo* (Miller et al., 2013). Recently, a female patient from Netherlands having hip prosthesis and infected with *Candida albicans* was successfully treated using bone cement spacer impregnated with voriconazole and amphotericin B (Deelstra et al., 2013).

5.5. Biodegradable component

It is undeniable that PMMA has got enormous popularity among the surgeons as the prosthetic devices for delivering the antibiotic loaded

beads. However, few drawbacks have prompted the researchers to look for other alternatives.

1. There always lies the need of a second surgical intervention for removal of PMMA based surgical devices.

2. Prolonged use of antibiotic at sub-therapeutic concentration may lead to the development of antibiotic resistance.

3. Chance of systemic toxicity leading to post-surgical hypotension due to absorbed monomers cannot be ignored.

4. Delayed bone healing due to use of PMMA based materials has been cited by many previous workers.

As alternatives, biodegradable materials were mostly used by the researchers. The duration of biodegradation vary depending upon status of infection and amount of tissue reconstruction/ repairing required. Using bio-degradable materials, tissue reconstruction or invasive tissue defect repairing interventions are not required at the extent what is required for acrylic based prosthetic devices. This is because; host soft tissues can fill the gaps what is left by slow absorption of the biodegradable beads. The antibiotic delivery system is also more effective using biodegradable elements. Using the PMMA system, antibiotic delivery is incomplete and complete removal of antibiotic is only possible with removal of the beads. Thus persistence release of antibiotics from the beads for the whole duration and its incomplete and variable delivery cannot be avoided. In contrast, use of biodegradable elements ensures a complete and effective delivery of the antibiotics.

Biodegradable elements can broadly divided in three groups –

1. Proteins
2. Bone graft materials and substitutes
3. Synthetic polymers

There are varieties of biological substances under proteins group of biodegradable elements. The group comprises of elements like, collagen, gelatin, thrombin and autologous blood clot.

Multiple bone graft substitutes were studied for their role as prosthetic implants/devices. Particularly, as a bone graft, morselized cancellous bone was extensively used for nearly twenty years. The antibiotics may be added to the bone graft by direct mixing of the antibiotic powder to the graft or the bone graft may be directly soaked in the antibiotic solution. Previous studies have indicated that antibiotics like tobramycin, netilmicin, vancomycin, clindamycin and rifampicin could be used with bone graft as a carrier and the antibiotics are released from the graft on the basis of first order kinetics. All the antibiotics maintained their bactericidal concentration for 1–3 weeks at the place of implant. Although, tobramycin is long used for impregnation, but it has shown delayed implant fixation (Gogia et al., 2009), which has been further substantiated in an experimental study in canines (Barckman et al., 2014). Autogenous bone graft is another substitute, which has long been used by the clinicians. Excellent recovery in patients with tibial fractures has been reported (Chan et al., 1998). Apart from calcium phosphate based hydroxyapatite or tricalcium phosphate, calcium sulfate was also used in management of osteomyelitis patients (Tsourvakas, 2012). A recent study has been carried out using ceftriaxone-sulbactam sodium loaded hydroxyapatite beads both *in vivo* animal model and final validation in human osteomyelitis patients with the observation of new osteogenesis and no sign of further bone infection in a study period of 8 months (Bhattacharya et al., 2013). Salient post-operative observations thus obtained are again reproduced in Figs. 4–5. There are certain advantages of using these materials. These materials can supply adequate antibiotic concentration at the site of interest and also accelerate the bone regeneration and healing process. Moreover, because of their low immune-reactivity, chance of adverse tissue reaction or hypersensitive tissue rejection reaction can be excluded out. The chance of transmitting infective pathogen as often noted in case of bone allograft can also be avoided using such biomaterials. Calcium

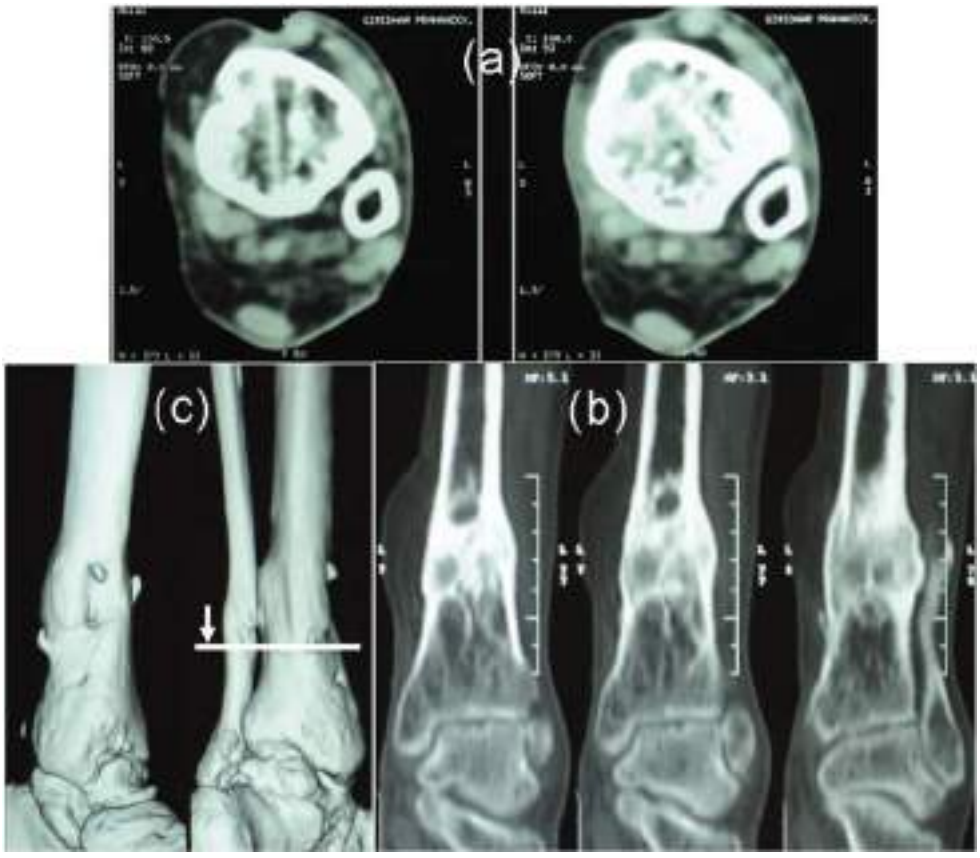

Fig. 5. Post-operative CT pictures of healed osteomyelitis bone. 2-dimensional CT studies of operated area in different cross sections (a), longitudinal sections (b) and its 3-dimensional reconstruction (c) performed after 8 months (with permissions from Elsevier).

Table 4
Antibiotic elution profile with local delivery system.

Antibiotics	Carrier	Concentration	Peak concentration	Time of peak	Duration	Reference
Rifampin	Acrylic bone cement	10%	15 mg/mL	3 day	>30 days	(Galvez-Lopez et al., 2014)
Moxifloxacin	Acrylic bone cement	10%	25 mg/mL	4 days	>30 days	
Daptomycin	Acrylic bone cement	10%	8–9 mg/mL	3–4 days	>30 days	
Cefotaxime	Acrylic bone cement	10%	13 mg/mL	1st day	>30 days	
Gentamycin	Acrylic bone cement		10 mg/mL	3rd day	>30 days	
Vancomycin	Acrylic bone cement	10%	32 mg/L	1st day	>30 days	
Etrapenem	Acrylic bone cement	10%	13 mg/mL	3 day	>30 days	
Meropenem	Acrylic bone cement	10%	13 mg/mL	1–2 days	>30 days	
Cefepime	Acrylic bone cement	10%	<2 mg mg/mL	2 day	8–9 day	
Ampicillin	Acrylic bone cement	10%	<2 mg/mL	2nd h	<5 days	
Meropenem	Simplex bone cement	10%	57.83 ± 7.45 μg/mL	1st h	20 days	(Samuel et al., 2012)
Cefazolin	Calcium sulfate	1 g of cefazolin	>1000 μg/mL	1st day	>15 days	(Udomkusonsri et al., 2012)
Penicillin			199.5 μg	1	91 days	(Nandi et al., 2009)
Tobramycin	β-tricalcium phosphate-silicate-xerogel		4 ppm	1	>9 days	
Ciprofloxacin	PMMA bone cement		74.5 mg/L	1	28 days	(Nandi et al., 2009; Tsourvakas et al., 2009;
			80.8 μg/mL		360 days	Wininger and Fass, 1996)
Clindamycin			407 mg/L	1	28 days	
Kanamycin			12.5 μg	1	8 days	(Nandi et al., 2009)
Cefazolin	…		250 mg/L		28 days	(Nandi et al., 2009)

sulfate and cancellous bone grafts are most commonly studied for this purpose. Calcium sulfate is being used for long for their low immune-reactivity, structural properties and easy reabsorption. Most common antibiotics used with calcium sulfate are vancomycin and tobramycin (1 and 1.25 g par 25 g of calcium sulfate). Application of tobramycin and vancomycin impregnated calcium sulphate was effective to reduce the chance of prosthetic infection. Such implant also prevented biofilm formation and colonization of the bacteria like MRSA and other CoNS. Recent studies conducted by McConoughey et al. revealed that calcium sulphate may perform as good as PMMA as carrier of antibiotics in orthopaedic infection (McConoughey et al., 2015). Both the antibiotic impregnated materials have displayed similar bactericidal property and similar kind of vancomycin elution. Another study confirmed that tobramycin loaded biodegradable calcium sulphate carrier may be useful in treatment of chronic osteomyelitis (Ferguson et al., 2014). With supplementation of 10 to 20 g of tobramycin impregnation, chance of renal toxicity is negligible in healthy persons. However, for patients with renal failure it may cause great concern (Ferguson et al., 2014).

Various protein based materials like antibiotic loaded sponge collagen, thrombin, fibrin and other clotted blood materials can be used for bone cementing. However, their use is very limited in management of orthopaedic infection. These materials provide a scaffold in and around the graft to limit the flow of fluid or provide the protein base for binding the antibiotic and thus the concentration of the drug and its sustained maintenance in the environment is ensured. Collagen based materials are usually prepared from skin or tendon of animals and can provide sufficient stimulation for bone regeneration with osteoblast proliferation and increased mineralization. Because collagen is found in almost in all organs as an elemental part of connective tissue, it is biologically desirable in the host with the graft and induces no toxicity. It's characteristic for drug content and elution can be modified by changing its porosity with chemical treatment. Recent studies using antibiotic loaded collagen sponges locally along with parenteral therapy show promising results in open fracture management (Chaudhary et al., 2010). Sternal wound is a serious complication following cardiac surgery and gentamicin loaded collagen sponge can be a good alternative for healing such wound (Bennett-Guerrero et al., 2010; Corn, 2010; Friberg et al., 2010). Fibrin sealants, the plasma homeostatic materials are also used for this purpose and have a great potential not only for management of orthopaedic and wound infection but also promote the tissue regeneration. Not only that the fibrin mass can also be degraded rapidly with plasma fibrinolysis (Mader et al., 2002). Fibrin sealants are more compatible with nonpolar antibiotics like tetracycline (Itokazu et al., 1997) (*cf.* Table 4).

(Galvez-Lopez et al., 2014; Nandi et al., 2009; Samuel et al., 2012; Tsourvakas et al., 2009; Udomkusonsri et al., 2012; Wininger and Fass, 1996).

5.6. Synthetic polymers

Biodegradable synthetic polymers are known to be used in surgical operation for long. However, these materials are also gaining popularity as local antibiotic delivery system among the clinicians for their lasting effects and antibiotic elution with increased penetrability in bone and soft tissue infection. Synthetic polymers are highly compatible with a number of antibiotics like ampicillin, gentamicin and polymixin-B. Polymers of lactide and glycolide are generally used for this purpose. Among other materials as synthetic polymers are polyhydride and polycaprolactones. Copolymers of polylactide and polyglycolide (90:10) are also used for their better compatibility with antibiotics like tobramycin, clindamycin and vancomycin (Billon et al., 2005). These materials are degraded very slowly over a long period of time only at physiological pH and thus can provide sustained release of antibiotics. Not only that, drug elution kinetics from these synthetic polymers can be modulated by changing physical, biochemical and molecular structural properties of the polymers (Barber and Hrnack, 2013).

Bio-absorbable gels containing antibiotics were found to offer rapid recovery rate than bone cement. Recent studies show significant reduction of infection rate using bio-absorbable gels containing antibiotics like gentamicin and vancomycin or with no antibiotics at all ($P < 0.001$) in an experimental open fracture model (Penn-Barwell et al., 2014). Both biodegradable and nonbiodegradable carrier system of local antibiotic delivery have been presented in Table 5.

(Alvarez et al., 2008; Ambrose et al., 2004; Brin et al., 2008; Ding et al., 2014; Drago et al., 2013; Ferguson et al., 2014; Garvin et al., 1994; Gursel et al., 2000; Jiang et al., 2012; Joosten et al., 2004; Joosten et al., 2005; Kanellakopoulou et al., 2009; Korkusuz et al., 1993; Krasko et al., 2007; Kundu et al., 2011; Kundu et al., 2010; Lian et al., 2015; Makinen et al., 2005; Miyai et al., 2008; Nelson et al., 2002; Riegels-Nielsen et al., 1995; Shirtliff et al., 2002; Vester et al., 2010; Wu et al., 2013; Xie et al., 2013; Xie et al., 2011; Xie et al., 2009; Zhang et al., 2010).

6. Conclusions

The proper use of antimicrobial agents is of paramount importance to reduce morbidity from osteomyelitis. Antibiotic therapy (either

Table 5
Antibiotic delivery materials locally.

Class	Material used	Antibiotic	microorganisms tested	Animal/human	Reference
Bioceramic	Calcium phosphate	Gentamicin	*S. aureus*	Rabbits	(Joosten et al., 2004)
	b-tricalcium phosphate	Gentamicin	*S. aureus*	Rat	(Wu et al., 2013)
	Calcium sulphate	Moxifloxacin	MRSA	Rabbits	(Kanellakopoulou et al., 2009)
	Calcium sulphate	Tobramycin sulphate	Chronic osteomyelitis	Human	(Ferguson et al., 2014)
	Calcium sulphate	Tobramycin sulphate	*S. aureus*	Rabbits	(Nelson et al., 2002)
	Hydroxyapatite	Ceftriaxone-sulbactam composite	*S. aureus*	Rabbits	(Kundu et al., 2010)
	Nano-hydroxyapatite pellets	Vancomycin	MRSA	Rabbits	(Jiang et al., 2012)
	Hydroxyapatite	Vancomycin	*S. aureus*	Rabbits	(Shirtliff et al., 2002)
	Hydroxyapatite	Gentamicin sulphate	*S. aureus*	Rats	(Korkusuz et al., 1993)
	Hydroxyapatite	Vancomycin	MRSA	Rabbits	(Joosten et al., 2005)
Polymer	Poly(d,l-lactide) (PDLLA)	Gentamicin	*S. aureus*	Rats	(Vester et al., 2010)
	Collagen	Gentamicin	*S. aureus*	Rabbits	(Riegels-Nielsen et al., 1995)
	PEG, PLGA	Tobramycin, Cefazolin	*S. aureus*	Rabbits	(Ambrose et al., 2004)
	Polyhydroxy-alkanoate	Sulbactam, cefoperazone, ampicillin	*S. aureus*	Rabbits	(Gursel et al., 2000)
	Polylactide/polyglicolide	Gentamicin	*S. aureus*	Dogs	(Garvin et al., 1994)
	P(SA-RA)	Gentamicin	*S. aureus*	Rats	(Brin et al., 2008)
	P(SA-RA)	Gentamicin	*S. aureus*	Rats	(Krasko et al., 2007)
Bioactive glass	Borate bioactive glass (BBG)	Gentamicin	*Escherichia coli*	Rabbit	(Xie et al., 2013)
	Borate	Vancomycin	MRSA	Rabbits	(Xie et al., 2011)
	Bioglass (BAG, S53P4)	–	MRSA and *S. epidermidis*, *P. aeruginosa* and *Acinetobacter baumannii*	Human	(Drago et al., 2013)
	Borate bioactive glass (BBG)	Teicoplanin	MRSA	Rabbit	(Zhang et al., 2010)
	Borate	Vancomycin	MRSA	Rabbits	(Xie et al., 2009)
	Boro-silicate	Ceftriaxone-sulbactam	*S. aureus*	Rabbits	(Kundu et al., 2011)
Composite	Nano-hydroxyapatite/collagen/calcium sulphate hemihydrate (nHAC/CSH)	Vancomycin	Chronic osteomyelitis	Rabbits	(Lian et al., 2015)
	Chitosan, borate glass	Teicoplanin	*S. aureus*	Rabbits	(Zhang et al., 2010)
	Chitosan-bonded borate bioactive glass	Vancomycin	MRSA	Rabbits	(Ding et al., 2014)
	PLGA, bioactive glass	Ciprofloxacin	*S. aureus, S. epidermidis, E. coli, P. aeruginosa*	Rabbits	(Makinen et al., 2005)
	Poly(D,L-lactide), tricalcium-phosphate, hydroxyapatite	Ciprofloxacin	*S. aureus*	Rabbits	(Alvarez et al., 2008)
	Poly-ε-caprolactone, tricalcium phosphate	Gatifloxacine	*S. milleri*, *B. fragilis*	Rabbits	(Miyai et al., 2008)

parenteral or oral route) was the conventional basis for management of this situation. Widespread research has been initiated to treat this situation through local drug delivery systems. Local antibiotic delivery system provides increase tissue concentration, less toxicity, and high efficacy. Antibiotic loaded non-biodegradable carrier has been successfully used in a number of applications, but these are needed to be removed through a second surgery. Local antibiotic delivery system using biodegradable materials especially from calcium phosphate based carriers not only deliver drug in the site of interest at a sustained level but also act as a bone filler material. Even though, it is of paramount necessity to explore proper biodegradable and biocompatible materials, the release kinetics and their bio-availability before many of these formulations can be used. The paucity of suitable *in vivo* trials in animal model makes their evaluation difficult. Recently, research has been initiated utilizing composite biocompatible and biodegradable materials as carrier system of antibiotic in treatment of osteomyelitis. In both ways, it will serve the purpose of releasing antibiotics at constant rates over long time and limit the multiple dosing. Still research has been limited within the material development and experimental animal trial. Limited data are available on using these new modalities in bed side in animal and human osteomyelitis patient which needs considerable attention. Development of new delivery systems in coming days would not only reduce the cost of treatment but also fulfill the patient's need.

Conflict of interest

The authors do not have conflict of interest.

Acknowledgement

The authors gratefully acknowledge the support by the Vice Chancellor, West Bengal Universityof Animal and Fishery Sciences, Kolkata, India; Director, CSIR-Central Glass and CeramicResearch Institute, Kolkata, India. Financial support of Council of Scientific and Industrial Research (CSIR) [through CSIR12th five year plan programme (BIOCERAM) ESC0103] is also thankfully acknowledged.

References

Al-Nawas, B., Kinzig-Schippers, M., Soergel, F., Shah, P.M., 2008. Concentrations of piperacillin-tazobactam in human jaw and hip bone. J. Cranio-Maxillofac. Surg. 36 (8), 468–472.

Alvarez, H., Castro, C., Moujir, L., Perera, A., Delgado, A., Soriano, I., Evora, C., Sanchez, E., 2008. Efficacy of ciprofloxacin implants in treating experimental osteomyelitis. J. Biomed. Mater. Res. B Appl. Biomater. 85 (1), 93–104.

Ambrose, C.G., Clyburn, T.A., Louden, K., Joseph, J., Wright, J., Gulati, P., Gogola, G.R., Mikos, A.G., 2004. Effective treatment of osteomyelitis with biodegradable microspheres in a rabbit model. Clin. Orthop. Relat. Res. 421, 293–299.

Anal, A.K., Stevens, W.F., 2005. Chitosan-alginate multilayer beads for controlled release of ampicillin. Int. J. Pharm. 290 (1), 45–54.

Arias, P.P., Tafin, U.F., Betrisey, B., Vogt, S., Trampuz, A., Borens, O., 2015. Activity of bone cement loaded with daptomycin alone or in combination with gentamicin or PEG600 against *Staphylococcus epidermidis* biofilms. Injury 46 (2), 249–253.

Baker, G.L., Oddis, C.V., Medsger Jr., T.A., 1987. Pasteurella multocida polyarticular septic arthritis. J. Rheumatol. 14 (2), 355–357.

Barber, F.A., Hrnack, S.A., 2013. Poly L-lactide co-glycolide/β-tricalcium phosphate interference screw fixation for bone-patellar tendon bone anterior cruciate ligament reconstruction. Journal of Knee Surgery 26 (6), 423–428.

Barckman, J., Baas, J., Sorensen, M., Lange, J., Bechtold, J.E., Soballe, K., 2014. Does tobramycin impregnation of allograft bone affect implant fixation? — An experimental study in 12 dogs. J. Biomed. Mater. Res. B Appl. Biomater. 102 (1), 173–180.

Baum, H.V., Bottcher, S., Abel, R., Gerner, H.J., Sonntag, H.G., 2001. Tissue and serum concentrations of levofloxacin in orthopaedic patients. Int. J. Antimicrob. Agents 18 (4), 335–340.

Bennett-Guerrero, E., Ferguson, T.B., Lin, M., Garg, J., Mark, D.B., Scavo, V.A., Kouchoukos, N., Richardson, J.B., Pridgen, R.L., Corey, G.R., 2010. Effect of an implantable gentamicin-collagen sponge on sternal wound infections following cardiac surgery: a randomized trial. J. Am. Med. Assoc. 304 (7), 755–762.

Bergan, T., Solhaug, J.H., Soreide, O., Leinebo, O., 1985. Comparative pharmacokinetics of metronidazole and tinidazole and their tissue penetration. Scand. J. Gastroenterol. 20 (8), 945–950.

Bhattacharya, R., Kundu, B., Nandi, S.K., Basu, D., 2013. Systematic approach to treat chronic osteomyelitis through localized drug delivery system: bench to bed side. Mater. Sci. Eng. C 33 (7), 3986–3993.

Billon, A., Chabaud, L., Gouyette, A., Bouler, J.M., Merle, C., 2005. Vancomycin biodegradable poly (lactide-co-glycolide) microparticles for bone implantation. Influence of the formulation parameters on the size, morphology, drug loading and in vitro release. J. Microencapsul. 22 (8), 841–852.

Bradley, J.S., Benziger, D., Bokesch, P., Jacobs, R., 2014. Single-dose pharmacokinetics of daptomycin in pediatric patients 3–24 months of age. Pediatr. Infect. Dis. J. 33 (9), 936–939.

Breilh, D., Boselli, E., Bel, J.C., Chassard, D., Saux, M.C., Allaouchiche, B., 2003. Diffusion of cefepime into cancellous and cortical bone tissue. J. Chemother. 15 (2), 134–138.

Brin, Y.S., Golenser, J., Mizrahi, B., Maoz, G., Domb, A.J., Peddada, S., Tuvia, S., Nyska, A., Nyska, M., 2008. Treatment of osteomyelitis in rats by injection of degradable polymer releasing gentamicin. J. Control. Release 131 (2), 121–127.

Calderini, C., Cioni, F., Haddoub, S., Maccanelli, F., Magotti, M.G., Tardio, S., 2014. Therapeutic approach to "diabetic foot" complications. Acta Bio Medica Atenei Parmensis 85 (3), 189–204.

Carmody, O., Cawley, D., Dodds, M., Connolly, P., 2014. Acute haematogenous osteomyelitis in children. Ir. Med. J. 107 (9), 269–270.

Catelas, I., Sese, N., Wu, B.M., Dunn, J.C.Y., Helgerson, S.A.M., Tawil, B., 2006. Human mesenchymal stem cell proliferation and osteogenic differentiation in fibrin gels in vitro. Tissue Eng. 12 (8), 2385–2396.

Chan, Y.-S., Ueng, S.W.-N., Wang, C.-J., Lee, S.-S., Chao, E.-K., Shin, C.-H., 1998. Management of small infected tibial defects with antibiotic-impregnated autogenic cancellous bone grafting. J. Trauma Acute Care Surg. 45 (4), 758–764.

Chandrasekar, P.H., Narula, A.P., 1986. Bone and joint infections in intravenous drug abusers. Rev. Infect. Dis. 8 (6), 904–911.

Chang, Y., Tai, C.L., Hsieh, P.H., Ueng, S.W.N., 2013. Gentamicin in bone cement A potentially more effective prophylactic measure of infection in joint arthroplasty. Bone and Joint Research 2 (10), 220–226.

Chaudhary, S., Sen, R.K., Saini, U.C., Soni, A., Gahlot, N., Singh, D., 2010. Use of gentamicin-loaded collagen sponge in internal fixation of open fractures. Chin. J. Traumatol. 14 (4), 209–214.

Chen, D.W., Chang, Y., Hsieh, P.-H., Ueng, S.W.N., Lee, M.S., 2013. The influence of storage temperature on the antibiotic release of vancomycin-loaded polymethylmethacrylate. Sci. World J. 2013, 573526.

Cios, A., Wyska, E., Szymura-Oleksiak, J., Grodzicki, T., 2014. Population pharmacokinetic analysis of ciprofloxacin in the elderly patients with lower respiratory tract infections. Exp. Gerontol. 57, 107–113.

Cooney, D.R., Cooney, N.L., 2011. Gas gangrene and osteomyelitis of the foot in a diabetic patient treated with tea tree oil. International Journal of Emergency Medicine 4 (1), 1–4.

Corn, T., 2010. Treating sternal wound infections after cardiac surgery with an implantable gentamicin-collagen sponge. J. Am. Med. Assoc. 304 (19), 2123–2124.

Deelstra, J.J., Neut, D., Jutte, P.C., 2013. Successful treatment of *Candida albicans*-infected total hip prosthesis with staged procedure using an antifungal-loaded cement spacer. J. Arthroplasty 28 (2), 374.e375–374.e378.

Ding, H., Zhao, C.-J., Cui, X., Gu, Y.-F., Jia, W.-T., Rahaman, M.N., Wang, Y., Huang, W.-H., Zhang, C.-Q., 2014. A novel injectable borate bioactive glass cement as an antibiotic delivery vehicle for treating osteomyelitis. PLoS One 9 (1), e85472.

Drago, L., Romano, D., De Vecchi, E., Vassena, C., Logoluso, N., Mattina, R., Romano, C.L., 2013. Bioactive glass BAG-S53P4 for the adjunctive treatment of chronic osteomyelitis of the long bones: an in vitro and prospective clinical study. BMC Infect. Dis. 13 (1), 584.

Eid, A.J., Berbari, E.F., 2011. Osteomyelitis: review of pathophysiology, diagnostic modalities and therapeutic options. The Lebanese Medical Journal 60 (1), 51–60.

Falagas, M.E., Siempos, I.I., Papagelopoulos, P.J., Vardakas, K.Z., 2007. Linezolid for the treatment of adults with bone and joint infections. Int. J. Antimicrob. Agents 29 (3), 233–239.

Ferguson, J.Y., Dudareva, M., Riley, N.D., Stubbs, D., Atkins, B.L., McNally, M.A., 2014. The use of a biodegradable antibiotic-loaded calcium sulphate carrier containing tobramycin for the treatment of chronic osteomyelitis a series of 195 cases. Bone and Joint Journal 96 (6), 829–836.

Fish, D.N., Chow, A.T., 1997. The clinical pharmacokinetics of levofloxacin. Clin. Pharmacokinet. 32 (2), 101–119.

Frank, D., Montsko, G., Juricskay, I., Borsiczky, B., Cseh, G., Kocsis, B., Nagy, T., Nagy, A.K., Kovacs, G.L., Miseta, A., 2011. Clindamycin release determined by high performance liquid chromatography from a novel low-cost local drug delivery system: a new potential treatment option for chronic osteomyelitis. J. Chemother. 23 (5), 282–284.

Friberg, O., Svedjeholm, R., Soderquist, B., 2010. Treating sternal wound infections after cardiac surgery with an implantable gentamicin-collagen sponge. J. Am. Med. Assoc. 304 (19), 2123–2124.

Galvez-Lopez, R., Pena-Monje, A., Antelo-Lorenzo, R., Guardia-Olmedo, J., Moliz, J., Hernandez-Quero, J., Parra-Ruiz, J., 2014. Elution kinetics, antimicrobial activity, and mechanical properties of 11 different antibiotic loaded acrylic bone cement. Diagn. Microbiol. Infect. Dis. 78 (1), 70–74.

Garazzino, S., Aprato, A., Baietto, L., D'Avolio, A., Maiello, A., De Rosa, F.G., Aloj, D., Siccardi, M., Biasibetti, A., Masse, A., 2008. Glycopeptide bone penetration in patients with septic pseudoarthrosis of the tibia. Clin. Pharmacokinet. 47 (12), 793–805.

Garazzino, S., Aprato, A., Baietto, L., D'Avolio, A., Maiello, A., De Rosa, F.G., Aloj, D., Siccardi, M., Biasibetti, A., Masse, A., 2011. Ceftriaxone bone penetration in patients with septic non-union of the tibia. Int. J. Infect. Dis. 15 (6), e415–e421.

Garvin, K.L., Miyano, J.A., Robinson, D., Giger, D., Novak, J., Radio, S., 1994. Polylactide/polyglycolide antibiotic implants in the treatment of osteomyelitis. A canine model. J. Bone Joint Surg. Am. 76 (10), 1500–1506.

Gnarpe, H., Dornbusch, K., Hagg, O., 1976. Doxycycline concentration levels in bone, soft tissue and serum after intravenous infusion of doxycycline. Scand. J. Infect. Dis. 8 (Supplement 9), 54–57.

Gogia, J.S., Meehan, J.P., Di Cesare, P.E., Jamali, A.A., 2009. Local antibiotic therapy in osteomyelitis. Semin. Plast. Surg. 100–107.

Goss, B., Lutton, C., Weinrauch, P., Jabur, M., Gillett, G., Crawford, R., 2007. Elution and mechanical properties of antifungal bone cement. J. Arthroplast. 22 (6), 902–908.

Goudah, A., Hasabelnaby, S., 2010. Pharmacokinetics, plasma protein binding and bioavailability of moxifloxacin in Muscovy ducks after different routes of administration. Res. Vet. Sci. 88 (3), 507–511.

Gould, I.M., David, M.Z., Esposito, S., Garau, J., Lina, G., Mazzei, T., Peters, G., 2012. New insights into meticillin-resistant *Staphylococcus aureus* (MRSA) pathogenesis, treatment and resistance. Int. J. Antimicrob. Agents 39 (2), 96–104.

Graziani, A.L., Lawson, L.A., Gibson, G.A., Steinberg, M.A., MacGregor, R.R., 1988. Vancomycin concentrations in infected and noninfected human bone. Antimicrob. Agents Chemother. 32 (9), 1320–1322.

Gursel, I., Korkusuz, F., Turesin, F., Alaeddinoglu, N.G., Hasirci, V., 2000. In vivo application of biodegradable controlled antibiotic release systems for the treatment of implant-related osteomyelitis. Biomaterials 22 (1), 73–80.

Haas, D.W., McAndrew, M.P., 1996. Bacterial osteomyelitis in adults: evolving considerations in diagnosis and treatment. Am. J. Med. 101 (5), 550–561.

Hanssen, A.D., Spangehl, M.J., 2004. Treatment of the infected hip replacement. Clin. Orthop. Relat. Res. 420, 63–71.

Hartwig, N.G., 2006. How to treat acute musculoskeletal infections in children. Hot Topics in Infection and Immunity in Children III. Springer, pp. 191–200.

Herrmann, M., Vaudaux, P.E., Pittet, D., Auckenthaler, R., Lew, P.D., Perdreau, F.S., Peters, G., Waldvogel, F.A., 1988. Fibronectin, fibrinogen, and laminin act as mediators of adherence of clinical staphylococcal isolates to foreign material. J. Infect. Dis. 158 (4), 693–701.

Hsu, Y.-M., Liao, C.-H., Wei, Y.-H., Fang, H.-W., Hou, H.-H., Chen, C.-C., Chang, C.-H., 2014. Daptomycin-loaded polymethylmethacrylate bone cement for joint arthroplasty surgery. Artif. Organs 38 (6), 484–492.

Insall, J.N., Thompson, F.M., Brause, B.D., 2002. Two-stage reimplantation for the salvage of infected total knee arthroplasty. J. Bone Joint Surg. Am. 84 (3), 490.

Itokazu, M., Yamamoto, K., Yang, W.Y., Aoki, T., Kato, N., Watanabe, K., 1997. The sustained release of antibiotic from freeze-dried fibrin-antibiotic compound and efficacies in a rat model of osteomyelitis. Infection 25 (6), 359–363.

Javaloyas, d.M.M., Monreal, P.M., 1999. Oral antibiotic therapy in the adult bacterial osteomyelitis: results after two years of follow-up. Med. Clin. 113 (13), 488–489.

Jiang, J.-L., Li, Y.-F., Fang, T.-L., Zhou, J., Li, X.-L., Wang, Y.-C., Dong, J., 2012. Vancomycin-loaded nano-hydroxyapatite pellets to treat MRSA-induced chronic osteomyelitis with bone defect in rabbits. Inflamm. Res. 61 (3), 207–215.

Joosten, U., Joist, A., Frebel, T., Brandt, B., Diederichs, S., Von Eiff, C., 2004. Evaluation of an in situ setting injectable calcium phosphate as a new carrier material for gentamicin in the treatment of chronic osteomyelitis: studies in vitro and in vivo. Biomaterials 25 (18), 4287–4295.

Joosten, U., Joist, A., Gosheger, G., Liljenqvist, U., Brandt, B., von Eiff, C., 2005. Effectiveness of hydroxyapatite-vancomycin bone cement in the treatment of *Staphylococcus aureus* induced chronic osteomyelitis. Biomaterials 26 (25), 5251–5258.

Joyner, A.L., Smith, D.T., 1936. Acute staphylococcus osteomyelitis. Surg. Gynecol. Obstet. 63, 1–6.

Kanellakopoulou, K., Galanopoulos, I., Soranoglou, V., Tsaganos, T., Tziortzioti, V., Maris, I., Papalois, A., Giamarellou, H., Giamarellos-Bourboulis, E.J., 2009. Treatment of experimental osteomyelitis caused by methicillin-resistant *Staphylococcus aureus* with a synthetic carrier of calcium sulphate (Stimulan®) releasing moxifloxacin. Int. J. Antimicrob. Agents 33 (4), 354–359.

King, R.W., 2015. Osteomyelitis in Emergency Medicine. http://emedicine.medscape.com/article/785020-overview (accessed September 29).

Korkusuz, F., Uchida, A., Shinto, Y., Araki, N., Inoue, K., Ono, K., 1993. Experimental implant-related osteomyelitis treated by antibiotic-calcium hydroxyapatite ceramic composites. J. Bone Joint Surg. (Br.) 75 (1), 111–114.

Krasko, M.Y., Golenser, J., Nyska, A., Nyska, M., Brin, Y.S., Domb, A.J., 2007. Gentamicin extended release from an injectable polymeric implant. J. Control. Release 117 (1), 90–96.

Kundu, B., Soundrapandian, C., Nandi, S.K., Mukherjee, P., Dandapat, N., Roy, S., Datta, B.K., Mandal, T.K., Basu, D., Bhattacharya, R., 2010. Development of new localized drug delivery system based on ceftriaxone-sulbactam composite drug impregnated porous hydroxyapatite: a systematic approach for in vitro and in vivo animal trial. Pharm. Res. 27 (8), 1659–1676.

Kundu, B., Nandi, S.K., Dasgupta, S., Datta, S., Mukherjee, P., Roy, S., Singh, A.K., Mandal, T.K., Das, P., Bhattacharya, R., 2011. Macro-to-micro porous special bioactive glass and ceftriaxone-sulbactam composite drug delivery system for treatment of chronic osteomyelitis: an investigation through in vitro and in vivo animal trial. J. Mater. Sci. Mater. Med. 22 (3), 705–720.

Kutscha-Lissberg, F., Hebler, U., Muhr, G., Koller, M., 2003. Linezolid penetration into bone and joint tissues infected with methicillin-resistant staphylococci. Antimicrob. Agents Chemother. 47 (12), 3964–3966.

Lalidou, F., Kolios, G., Drosos, G.I., 2014. Bone infections and bone graft substitutes for local antibiotic therapy. Surg. Technol. Int. 24, 353–362.

Landersdorfer, C.B., Kinzig, M., Hennig, F.F., Bulitta, J.B., Holzgrabe, U., Drusano, G.L., Sorgel, F., Gusinde, J., 2009. Penetration of moxifloxacin into bone evaluated by Monte Carlo simulation. Antimicrob. Agents Chemother. 53 (5), 2074–2081.

Lew, D.P., Waldvogel, F.A., 2004. Osteomyelitis. Lancet 364 (9431), 369–379.

Lewis, G., 2009. Properties of antibiotic-loaded acrylic bone cements for use in cemented arthroplasties: a state-of-the-art review. J. Biomed. Mater. Res. B Appl. Biomater. 89 (2), 558–574.

Lian, X., Mao, K., Liu, X., Wang, X., Cui, F., 2015. In vivo osteogenesis of vancomycin loaded nanohydroxyapatite/collagen/calcium sulfate composite for treating infectious bone defect induced by chronic osteomyelitis. J. Nanomater. 2015, 13.

Lindfors, N.C., Hyvonen, P., Nyyssonen, M., Kirjavainen, M., Kankare, J., Gullichsen, E., Salo, J., 2010. Bioactive glass S53P4 as bone graft substitute in treatment of osteomyelitis. Bone 47 (2), 212–218.

Lovering, A.M., Walsh, T.R., Bannister, G.C., MacGowan, A.P., 2001. The penetration of ceftriaxone and cefamandole into bone, fat and haematoma and relevance of serum protein binding to their penetration into bone. J. Antimicrob. Chemother. 47 (4), 483–486.

Lu, P.L., Wang, J.T., Chen, C.J., Chen, W.C., Chen, T.C., Hwang, Y.C., Chang, S.C., 2010. Compassionate use of linezolid for adult Taiwanese patients with bone and joint infections. Chemotherapy 56 (6), 429–435.

Mader, J.T., Shirtliff, M., Calhoun, J.H., 1999a. The host and the skeletal infection: classification and pathogenesis of acute bacterial bone and joint sepsis. Best Pract. Res. Clin. Rheumatol. 13 (1), 1–20.

Mader, J.T., Shirtliff, M.E., Bergquist, S.C., Calhoun, J., 1999b. Antimicrobial treatment of chronic osteomyelitis. Clin. Orthop. Relat. Res. 360, 47–65.

Mader, J.T., Stevens, C.M., Stevens, J.H., Ruble, R., Lathrop, J.T., Calhoun, J.H., 2002. Treatment of experimental osteomyelitis with a fibrin sealant antibiotic implant. Clin. Orthop. Relat. Res. 403, 58–72.

Magnan, B., Bondi, M., Maluta, T., Samaila, E., Schirru, L., Dall'Oca, C., 2013. Acrylic bone cement: current concept review. Musculoskelet. Surg. 97 (2), 93–100.

Makinen, T.J., Veiranto, M., Lankinen, P., Moritz, N., Jalava, J., Tormala, P., Aro, H.T., 2005. In vitro and in vivo release of ciprofloxacin from osteoconductive bone defect filler. J. Antimicrob. Chemother. 56 (6), 1063–1068.

Malincarne, L., Ghebregzabher, M., Moretti, M.V., Egidi, A.M., Canovari, B., Tavolieri, G., Francisci, D., Cerulli, G., Baldelli, F., 2006. Penetration of moxifloxacin into bone in patients undergoing total knee arthroplasty. J. Antimicrob. Chemother. 57 (5), 950–954.

Marchocki, Z., Collins, K., Lehane, E., O'Reilly, P., O'Donoghue, K., 2013. Staphylococcus lugdunensis cultured from the amniotic fluid at caesarean section. PLoS One 8 (2), e56373.

Maxe, I., Ryden, C., Wadstrom, T., Rubin, K., 1986. Specific attachment of *Staphylococcus aureus* to immobilized fibronectin. Infect. Immun. 54 (3), 695–704.

McConoughey, S.J., Howlin, R.P., Wiseman, J., Stoodley, P., Calhoun, J.H., 2015. Comparing PMMA and calcium sulfate as carriers for the local delivery of antibiotics to infected surgical sites. J. Biomed. Mater. Res. B Appl. Biomater. 103 (4), 870–877.

Metallidis, S., Charokopos, N., Nikolaidis, J., Alexiadou, E., Lazaraki, G., Koumentaki, E., Tsona, A., Theodoridis, G., Nikolaidis, P., 2006. Penetration of moxifloxacin into sternal bone of patients undergoing routine cardiopulmonary bypass surgery. Int. J. Antimicrob. Agents 28 (5), 428–432.

Metallidis, S., Topsis, D., Nikolaidis, J., Alexiadou, E., Lazaraki, G., Grovaris, L., Theodoridou, A., Nikolaidis, P., 2007. Penetration of moxifloxacin and levofloxacin into cancellous and cortical bone in patients undergoing total hip arthroplasty. J. Chemother. 19 (6), 682–687.

Miller, R.B., McLaren, A.C., Pauken, C., Clarke, H.D., McLemore, R., 2013. Voriconazole is delivered from antifungal-loaded bone cement. Clin. Orthop. Relat. Res. 471 (1), 195–200.

Miyai, T., Ito, A., Tamazawa, G., Matsuno, T., Sogo, Y., Nakamura, C., Yamazaki, A., Satoh, T., 2008. Antibiotic-loaded poly-ε-caprolactone and porous β-tricalcium phosphate composite for treating osteomyelitis. Biomaterials 29 (3), 350–358.

Montange, D., Berthier, F., Leclerc, G., Serre, A., Jeunet, L., Berard, M., Muret, P., Vettoretti, L., Leroy, J., Hoen, B., 2014. Penetration of daptomycin into bone and synovial fluid in joint replacement. Antimicrob. Agents Chemother. 58 (7), 3991–3996.

Nandi, S.K., Mukherjee, P., Roy, S., Kundu, B., De, D.K., Basu, D., 2009. Local antibiotic delivery systems for the treatment of osteomyelitis — a review. Mater. Sci. Eng. C 29 (8), 2478–2485.

Nelson, C.L., McLaren, S.G., Skinner, R.A., Smeltzer, M.S., Thomas, J.R., Olsen, K.M., 2002. The treatment of experimental osteomyelitis by surgical debridement and the implantation of calcium sulfate tobramycin pellets. J. Orthop. Res. 20 (4), 643–647.

Nguyen, S., Pasquet, A., Legout, L., Beltrand, E., Dubreuil, L., Migaud, H., Yazdanpanah, Y., Senneville, E., 2009. Efficacy and tolerance of rifampicin-linezolid compared with rifampicin-cotrimoxazole combinations in prolonged oral therapy for bone and joint infections. Clin. Microbiol. Infect. 15 (12), 1163–1169.

Patti, J.M., Boles, J.O., Hook, M., 1993. Identification and biochemical characterization of the ligand binding domain of the collagen adhesin from *Staphylococcus aureus*. Biochemistry 32 (42), 11428–11435.

Patzakis, M.J., Wilkins, J., 1989. Factors influencing infection rate in open fracture wounds. Clin. Orthop. Relat. Res. 243, 36–40.

Patzakis, M.J., Zalavras, C.G., 2005. Chronic posttraumatic osteomyelitis and infected nonunion of the tibia: Current management concepts. J. Am. Acad. Orthop. Surg. 13 (6), 417–427.

Penn-Barwell, J.G., Murray, C.K., Wenke, J.C., 2014. Local antibiotic delivery by a bioabsorbable gel is superior to PMMA bead depot in reducing infection in an open fracture model. J. Orthop. Trauma 28 (6), 370–375.

Philippe Bidault, D.C.D., Chandad, F., Grenier, D., 2007. Risk of bacterial resistance associated with systemic antibiotic therapy in periodontology. J. Can. Dent. Assoc. 73 (8), 721–725.

Phillips, J.E., Crane, T.P., Noy, M., Elliott, T.S.J., Grimer, R.J., 2006. The incidence of deep prosthetic infections in a specialist orthopaedic hospital: a 15-year prospective surgery. J. Bone Joint Surg. Br. Vol. 88 (7), 943–948.

Pithankuakul, K., Samranvedhya, W., Visutipol, B., Rojviroj, S., 2015. The effects of different mixing speeds on the elution and strength of high-dose antibiotic-loaded bone cement created with the hand-mixed technique. J. Arthroplast. 30 (5), 858–863.

Rana, B., Butcher, I., Grigoris, P., Murnaghan, C., Seaton, R.A., Tobin, C.M., 2002. Linezolid penetration into osteo-articular tissues. J. Antimicrob. Chemother. 50 (5), 747–750.

Raymakers, J.T., Schaper, N.C., Van Der Heyden, J.J., Tordoir, J.H., Kitslaar, P.J., 1998. Penetration of ceftazidime into bone from severely ischaemic limbs. J. Antimicrob. Chemother. 42 (4), 543–545.

Regis, D., Sandri, A., Samaila, E., Benini, A., Bondi, M., Magnan, B., 2013. Release of gentamicin and vancomycin from preformed spacers in infected total hip arthroplasties: measurement of concentrations and inhibitory activity in patients' drainage fluids and serum. Sci. World J. 2013, 752184.

Rick, D., Anthony, M., Julia, A., 1996. Ciprofloxacin. An updated review of its pharmacology therapeutic efficacy and tolerability. Drugs 51, 1019–1074.

Riegels-Nielsen, P., Espersen, F., Holmich, L.R., Frimodt-moller, N., 1995. Collagen with gentamicin for prophylaxis of postoperative infection: *Staphylococcus aureus* osteomyelitis studied in rabbits. Acta Orthop. Scand. 66 (1), 69–72.

Rimmele, T., Boselli, E., Breilh, D., Djabarouti, S., Bel, J.C., Guyot, R., Saux, M.C., Allaouchiche, B., 2004. Diffusion of levofloxacin into bone and synovial tissues. J. Antimicrob. Chemother. 53 (3), 533–535.

Rushton, N., 1996. Applications of local antibiotic therapy. Eur. J. Surg. 27–30 Supplement(578).

Samuel, S., Mathew, B.S., Veeraraghavan, B., Fleming, D.H., Chittaranjan, S.B., Prakash, J.A.J., 2012. In vitro study of elution kinetics and bio-activity of meropenem-loaded acrylic bone cement. J. Orthop. Traumatol. 13 (3), 131–136.

Schintler, M.V., Traunmuller, F., Metzler, J., Kreuzwirt, G., Spendel, S., Mauric, O., Popovic, M., Scharnagl, E., Joukhadar, C., 2009. High fosfomycin concentrations in bone and peripheral soft tissue in diabetic patients presenting with bacterial foot infection. J. Antimicrob. Chemother. 64 (3), 574–578.

Schurman, D.J., Johnson Jr., B.L., Finerman, G., Amstutz, H.C., 1975. Antibiotic bone penetration: concentrations of methicillin and clindamycin phosphate in human bone taken during total hip replacement. Clin. Orthop. Relat. Res. 111, 142–146.

Shi, J., Mao, N.-F., Wang, L., Zhang, H.-B., Chen, Q., Liu, H., Tang, X., Jin, T., Zhu, C.-T., Li, F.-B., 2014. Efficacy of combined vancomycin and fosfomycin against methicillin-resistant *Staphylococcus aureus* in biofilms in vivo. PLoS One 9 (12), e113133.

Shirtliff, M.E., Calhoun, J.H., Mader, J.T., 2002. Experimental osteomyelitis treatment with antibiotic-impregnated hydroxyapatite. Clin. Orthop. Relat. Res. 401, 239–247.

Stass, H., Dalhoff, A., Kubitza, D., Schuhly, U., 1998. Pharmacokinetics, safety, and tolerability of ascending single doses of moxifloxacin, a new 8-methoxy quinolone, administered to healthy subjects. Antimicrob. Agents Chemother. 42 (8), 2060–2065.

Stein, G.E., Gurwith, D., Gurwith, M., 1988. Randomized clinical trial of rifampin-trimethoprim and sulfamethoxazole-trimethoprim in the treatment of localized urinary tract infections. Antimicrob. Agents Chemother. 32 (6), 802–806.

Swoboda, S., Helbig, L., Kommerell, M., Simank, H.G., Kees, F., Geiss, H.K., Hoppe-Tichy, T., Schroder, K., 2009. Bone tissue and plasma concentrations of linezolid and vancomycin in rabbits with prosthesis-related infection due to MRSA. Die Pharmazie-An International Journal of Pharmaceutical Sciences 64 (6), 407–409.

Tottrup, M., Hardlei, T.F., Bendtsen, M., Bue, M., Brock, B., Fuursted, K., Soballe, K., Birke-Sorensen, H., 2014. Pharmacokinetics of cefuroxime in porcine cortical and cancellous bone determined by microdialysis. Antimicrob. Agents Chemother. 58 (6), 3200–3205.

Tsourvakas, S., 2012. Local Antibiotic Therapy in the Treatment of Bone and Soft Tissue Infections. INTECH Open Access Publisher, Rijeka, Croatia.

Tsourvakas, S., Alexandropoulos, C., Karatzios, C., Egnatiadis, N., Kampagiannis, N., 2009. Elution of ciprofloxacin from acrylic bone cement and fibrin clot: an in vitro study. Acta Orthop. Belg. 75 (4), 537–542.

Udomkusonsri, P., Kaewmokul, S., Arthitvong, S., Phaochoosak, N., 2012. Elution profiles of cefazolin from PMMA and calcium sulfate beads prepared from commercial cefazolin formulations. J. Vet. Med. Sci. 74 (3), 301–305.

Vester, H., Wildemann, B., Schmidmaier, G., Stockle, U., Lucke, M., 2010. Gentamycin delivered from a PDLLA coating of metallic implants: In vivo and in vitro characterisation for local prophylaxis of implant-related osteomyelitis. Injury 41 (10), 1053–1059.

Waldvogel, F.A., Medoff, G., Swartz, M.N., 1970. Osteomyelitis: a review of clinical features, therapeutic considerations and unusual aspects. N. Engl. J. Med. 282 (4), 198–206.

Webb, J.C., Gbejuade, H., Lovering, A., Spencer, R., 2013. Characterisation of in vivo release of gentamicin from polymethyl methacrylate cement using a novel method. Int. Orthop. 37 (10), 2031–2036.

Weismeier, K., Adam, D., Heilmann, H.D., Koeppe, P., 1989. Penetration of amoxycillin/clavulanate into human bone. J. Antimicrob. Chemother. 24 (suppl B), 93–100.

Wilson, A.P.R., 2000. Clinical pharmacokinetics of teicoplanin. Clin. Pharmacokinet. 39 (3), 167–183.

Wininger, D.A., Fass, R.J., 1996. Antibiotic-impregnated cement and beads for orthopedic infections. Antimicrob. Agents Chemother. 40 (12), 2675–2679.

Wiskirchen, D.E., Shepard, A., Kuti, J.L., Nicolau, D.P., 2011. Determination of tissue penetration and pharmacokinetics of linezolid in patients with diabetic foot infections using in vivo microdialysis. Antimicrob. Agents Chemother. 55 (9), 4170–4175.
Wright, J.A., Nair, S.P., 2010. Interaction of staphylococci with bone. Int. J. Med. Microbiol. 300 (2), 193–204.
Wu, T., Zhang, Q., Ren, W., Yi, X., Zhou, Z., Peng, X., Yu, X., Lang, M., 2013. Controlled release of gentamicin from gelatin/genipin reinforced beta-tricalcium phosphate scaffold for the treatment of osteomyelitis. J. Mater. Chem. B 1 (26), 3304–3313.
Xie, Z., Liu, X., Jia, W., Zhang, C., Huang, W., Wang, J., 2009. Treatment of osteomyelitis and repair of bone defect by degradable bioactive borate glass releasing vancomycin. J. Control. Release 139 (2), 118–126.
Xie, Z., Liu, X., Jia, W., Zhang, C., Huang, W., 2011. Vancomycin-loaded bioactive borate glass for treatment of chronic osteomyelitis in rabbits. Chinese Journal of Reparative and Reconstructive Surgery 25 (7), 830–836.
Xie, Z., Cui, X., Zhao, C., Huang, W., Wang, J., Zhang, C., 2013. Gentamicin-loaded borate bioactive glass eradicates osteomyelitis due to *Escherichia coli* in a rabbit model. Antimicrob. Agents Chemother. 57 (7), 3293–3298.
Xing, J., Hou, T., Luobu, B., Luo, F., Chen, Q., Li, Z., Jin, H., Xu, J., 2012. Anti-infection tissue engineering construct treating osteomyelitis in rabbit tibia. Tissue Eng. A 19 (1–2), 255–263.
Zhang, X., Jia, W., Gu, Y., Xiao, W., Liu, X., Wang, D., Zhang, C., Huang, W., Rahaman, M.N., Day, D.E., 2010. Teicoplanin-loaded borate bioactive glass implants for treating chronic bone infection in a rabbit tibia osteomyelitis model. Biomaterials 31 (22), 5865–5874.

Glossary

*1. **Biofilm:** microorganisms/bacteria of any group rearrange themselves into cluster formation. These adherent cells embedding in a matrix have more tolerance to most antimicrobials as well as the host defense than planktonic bacterial cells.:*
*2. **Involucrum:** formation of thick sheath of periosteal new bone surrounding the infectious focus/sequestrum or abscess.:*
*3. **Planktonic phase:** apart from living as biofilms, bacterial also survive freely (contain <0.1% of the bacteria in the ecosystem) having all characteristics like reproduction, virulence, antibiotic sensitivity etc. This planktonic phase of bacteria can also be cultured.:*
*4. **Sequestrum:** fragment of dead bone separated during necrosis. It acts as a potential reservoir for infection (caused by bacteria and biofilm).:*
*5. **Sessile phase:** bacterial population existing in a slime layer, with low metabolic activity, controlled reproduction, hard to culture, tolerant to antibiotics and immune defenses.:*
*6. **Cancellous bone:** it is having light and porous structure, organized into a three-dimensional lattice work of bony processes, enclosing numerous large spaces that give a honeycombed or spongy appearance, also called trabecular bone or spongy bone.:*
*7. **Sialoglycoprotein:** a glycoprotein (which is itself, a combination of sugar and protein) having sialic acid as a component.:*
*8. **Prepubertal:** the period of life immediately before puberty when development of secondary sexual characteristics and the capability for reproduction begins.:*
*9. **Bone void filler**: it is a synthetic, osteoconductive material used as filler for gaps and voids in the extremities, spine, or pelvis. The voids are not essential for the stability of the bones.:*
*10. **Muscle hypertrophy:** the size of skeletal muscle is increased due to the increase of its surrounding component cells. Sarcoplasmic and myofibrillar hypertrophy are two major factors which focus on muscle glycogen storage and increased myofibril size respectively.:*
*11. **Metaphysis:** the epiphysis and the diaphysis are separated by the presence of a wide portion of a bone viz., metaphysic, considered to be a part of the growth plate or bone that grows during childhood and ossifies near the diaphysis and epiphyses.:*
*12. **Moth-eaten appearance:** the term describes the pattern of destruction. One kind of bone marrow process used to describe a permeative process of bone having multiple small endosteal lucent lesions or holes, often with poorly defined margins, with sparing of the cortex.:*
*13. **Bacteremia:** (also known as **bacteraemia**) is a bacterial infection in the blood.:*
*14. **Protease:** (also called proteolytic enzyme, **peptidase** or **proteinase**) can be described as a group of enzymes that hydrolyzes the protein into their building blocks viz. amino acids.:*
*15. **Peripheral neuropathy** (**PN**): it is a neurological disorder which may damage the act of sensation, movement and gland or organ function depending on the type of nerve affected.:*